

**Second-order constitutive relations and their topologies for rotational non-equilibrium in diatomic gas flows using a multi-temperature approach**

H. Srivastava (हर्षल श्रीवास्तव),<sup>1</sup> Tapan K. Mankodi (तपन के मंकोड़ी),<sup>1</sup> and R. S. Myong (명노신)<sup>2</sup>

<sup>1</sup>*Department of Mechanical Engineering, Indian Institute of Technology Guwahati, Guwahati, Assam 781039, India*

<sup>2</sup>*School of Mechanical and Aerospace Engineering, and ACTRC, Gyeongsang National University, Jinju, Gyeongnam 52828, South Korea*

(\*Electronic mail: myong@gnu.ac.kr)

(Dated: 4 March 2025)

## ABSTRACT

The phenomenon of rotational relaxation in diatomic gases such as nitrogen was studied in a non-equilibrium flow regime. Higher-order constitutive theory such as the nonlinear coupled constitutive relations (NCCR) approach was used to calculate the flow properties. The bulk viscosity-based approach, employing a single temperature to identify rotational non-equilibrium was found applicable for low Mach number cases. Since diatomic gases are characterized by additional degrees of freedom that may not be in equilibrium with each other in non-equilibrium flows, different temperatures need to be assigned to each degree of freedom to account for the same. Energy exchange between translational and rotational degrees of freedom was accomplished using the rotational energy equation with a non-zero source term. The source term was modeled using the Landau-Teller formulation and involved a rotational collision number representing the average number of collisions required to attain trans-rotational equilibrium. In the present work, it was calculated using the simplified formulation proposed by Parker. An additional non-conserved moment equation related to rotational heat flux was formulated under the NCCR framework and was solved in conjunction with other NCCR algebraic equations. It was noticed that the new two-temperature NCCR formulation for rotational non-equilibrium had better agreements with experiments, direct simulation Monte Carlo (DSMC), and molecular dynamics (MD) simulations. Moreover, the formulation was computationally less expensive than the DSMC/ MD simulations. A topological analysis was carried out to demonstrate the nonlinearity present in NCCR.

## I. INTRODUCTION

Diatomic gases are known to have internal degrees of freedom, such as rotational and vibrational degrees, that may not be in equilibrium in hypersonic flows. In such situations, an energy change in the domain is initially reflected by a change in translational energy and later gets re-distributed to other internal degrees of freedom. Generally, this redistribution of energy is quite fast, and the timescale is many orders of magnitude lower than the timescale of the flow. The flow in such cases is usually assumed to be in equilibrium and the distribution of energy follows the law of equipartition of energy.

However, in certain cases, such as the hypersonic flow around re-entry vehicles, the presence of high gradients and rarefied atmospheric conditions may delay the relaxation of internal energies to

such an extent that the flow time and relaxation time may become comparable. In such situations, the impact of the relaxation of internal energies and their redistribution may play a significant role in the flow physics.

Non-equilibrium phenomena in diatomic gases can be investigated using different approaches. The disparity in energy levels among various degrees of freedom can be modeled as an additional dissipative phenomenon, or by assuming a separate relaxation equation with different temperatures associated with each degree of freedom. This leads to the two basic approaches to the problem:

1. The single temperature approach with bulk viscosity accounting for internal modes, and
2. The multi-temperature relaxation equation approach.

The single-temperature formulation has the benefit of simplicity since it requires no additional accounting of the energy contents of different degrees of freedom. A property, known as bulk viscosity, is introduced in the momentum and the energy equations that account for the relaxation time associated with the internal degrees of freedom. The pressure tensor ( $\mathbf{P}$ ) is expanded to have a non-zero excess stress term ( $\Delta$ ), as given below.

$$\mathbf{P} = \mathbf{\Pi} + \Delta \mathbf{I} + p \mathbf{I} \quad (1)$$

where  $\mathbf{\Pi}$  is the stress term,  $p$  is the pressure, and  $\mathbf{I}$  is the identity matrix. While  $\Delta$  is zero for monoatomic gases, it may be non-zero for diatomic and polyatomic gases. It can be estimated using the first-order approximate formulation, which relates it to the bulk viscosity coefficient through the following relation.

$$\Delta = -\eta_b \nabla \cdot \mathbf{u} \quad (2)$$

where  $\eta_b$  is the coefficient of bulk viscosity and  $\mathbf{u}$  is the bulk velocity of the flow.

In the multi-temperature approach, additional energy equations for the internal degrees of freedom are included. The energy for various degrees of freedom is associated with a separate temperature value that may have a different value in the case of non-equilibrium flows. A source term is present that accounts for inter-mode energy transfer based on the temperature values of each degree of freedom. A typical evolution equation takes the following form.

$$\frac{\partial}{\partial t}(\rho E_m) + \nabla \cdot (E_m \mathbf{u}) + \nabla \cdot \mathbf{Q}_m = S_m \quad (3)$$

where  $\rho$  is the mass density,  $E_m$  is the energy per unit volume for the mode (m),  $\mathbf{Q}_m$  is the heat flux associated with the mode, and  $S_m$  is the source term.

It was shown by McCourt et al.<sup>1</sup> that the excess stress term,  $(\Delta)$ , appearing in the conservation laws is equivalent to the difference between the translational and rotational temperatures. Thus, the hydrodynamic equation can be formulated in two ways<sup>2,3</sup>: either by introducing the excess stress,  $(\Delta)$ , and retaining the one temperature ( $T_{trans-rot}$  or  $T_{t-r}$ ) concept, or by introducing translational ( $T_t$ ) and rotational ( $T_r$ ) temperatures and assuming no excess stress term. The former had been employed in previous studies<sup>4</sup> as it is a natural extension of the Navier-Stokes-Fourier (NSF) constitutive laws. Here we tried to explore the multi-temperature approach to the non-equilibrium problems.

The first attempt to modify the Boltzmann equation to include the rotational degree of freedom was carried out by Curtiss<sup>5</sup>. Curtiss employed the classical theory to model rigid convex non-spherical bodies having the center of mass at the center of symmetry. Chapman-Enskog theory (CE)<sup>6</sup> was employed, similar to the monoatomic gas flows. However, because of the complexities involved in the CE expansion, the resultant formulation was only applicable to a lower degree of non-equilibrium and for simple geometries.

Wang-Chang and Uhlenbeck<sup>7</sup> included the concepts of quantum mechanics with the Boltzmann equation with quantized levels of internal degrees, and obtained the semi-classical equations. The collision term was modified to incorporate transition probabilities for elastic, inelastic, and reactive transitions. Additionally, the Pauli exclusion principle was enforced, which restricted the transition to already occupied states.

Although Wang-Chang and Uhlenbeck were able to provide the formulation, the difficulty of solving the resultant set of equations was a major hindrance to its use in general cases. They specialized the formulation for two extreme cases, classified<sup>7</sup> as "when energy exchange between translational-internal degrees of freedom is not difficult" and "when the energy exchange is difficult". The first case involves the introduction of bulk viscosity to account for the lower degree of non-equilibrium, while the second case elucidates the importance of separate temperature values for the internal modes.

The bulk viscosity approach is central to the first case. As discussed earlier in the text, the minor deviation from equilibrium is modeled as additional viscous phenomena associated with the excess stress component in the pressure tensor. The second case involved relaxation phenomena and was modeled using a separate equation. However, the transport coefficients were in the form of

integrals having inelastic collision terms as integrands. Due to a lack of knowledge about inelastic collisions for any molecular model, further simplification could not be done.

For gases with internal degrees of freedom, a simplified model for the collision term, similar to the Bhatnagar-Gross-Krook (BGK) model of monoatomic gas, was formulated by Morse<sup>8</sup>. His model was based on the Wang-Chang and Uhlenbeck model for polyatomic gases. The two extreme cases were retaken and solved using this novel technique.

The BGK model offers extreme simplicity due to the simplified formulation of the collision term. However, the non-dimensional parameter such as the Prandtl number (Pr) calculated using the BGK model provides an incorrect value equal to 1 for monoatomic gases. An extension of the BGK model, to get the correct value of Pr, led to the development of the ES-BGK model<sup>9</sup>. The extension of the ES-BGK model to polyatomic gas involving rotational and vibrational equilibrium was carried out by Dauvois et al.<sup>10</sup>. They employed discrete vibrational energy levels for the study and subsequently proved the H-theorem for this model.

Rykov<sup>11</sup> proposed a new model kinetic equation considering the rotational degree of freedom in a diatomic gas. This model formed the basis of the numerical experiments, carried out by Rykov et al.<sup>12</sup> and Larina et al.<sup>13</sup>. Computed shock structures were in good agreement with experiments and DSMC simulations.

Contemporary to the above formulations, Curtiss<sup>14,15</sup> generalized his previous formulations to account for diatomic gases in general. His development considered diatomic gas as a special case. Further specialization to rigid-rotor and harmonic oscillator models was considered.

Recently, Wu et al.<sup>16</sup> implemented the Rykov model for inelastic collisions. The elastic collision was modeled using the Boltzmann collision operator (BCO), similar to that used for the monoatomic gas. The Boltzmann equation for monoatomic gases was obtained when the rotational contribution became zero. Shock waves in nitrogen gas were analyzed, and good agreements were observed with DSMC simulations.

Besides the kinetic model-based approach to non-equilibrium flows in diatomic gases, DSMC simulations were carried out by Bird<sup>17</sup> to predict shock structure in nitrogen gas. In a few cases, limited experimental results were also obtained by Alsmeyer<sup>18</sup>, Linzer et al.<sup>19</sup>. The DSMC and experimental results are often used to validate model kinetic equations and other computational methods.

Estimating the rotational collision number ( $Z_r$ ) is central to calculating the source term, required in a multi-temperature framework. It quantifies the average number of collisions required to attain

equilibrium between the internal and translational degrees of freedom. Various formulations were devised to calculate the rotational collision number. Parker<sup>20</sup> gave the first analytical formulation to calculate rotational and vibrational collision numbers. He obtained analytical expressions based on a simplified assumption, using the concepts of classical theory. He calculated rotational collision numbers<sup>21</sup> for various gases including  $Cl_2$ ,  $N_2$ , and  $O_2$ . His formulation predicted the strong dependence of the rotational collision numbers on the translational temperature. Parker's theoretical calculations were confirmed using ultrasonic experiments by Carnevale et al.<sup>22</sup>. They determined the rotational collision numbers and vibrational relaxation times of poly-atomic gases such as  $N_2$ ,  $O_2$ , and  $CO_2$ .

Parker had assumed certain restrictions for a colliding set of molecules, such as zero initial angular velocity and same-plane collision, and this resulted in an extremely idealized formulation. Nyeland<sup>23</sup> extended Parker's formulation by removing the assumption of zero angular velocity of colliding molecules. The result was, however, in poorer agreement with the experiments .

Valentini et al.<sup>24</sup> studied how the compression and expansion of gases affected the rotational collision number. They employed DSMC simulations to study shock structure and rarefaction and compared the results with MD and experimental data. A new fit to estimate  $Z_r$  was also proposed.

The present study incorporates a generalized hydrodynamics (GH) approach to solve the non-equilibrium phenomenon involving diatomic gases. The generalized hydrodynamics was developed by Eu<sup>25</sup>, as a modification to the moment method of Grad<sup>26,27</sup>. Eu assumed a special form for the probability distribution function that led to a more intuitive definition of entropy production<sup>28</sup>. The formulation strictly follows the second law of thermodynamics even at higher order approximations, which was a major drawback of the Chapman-Enskog formulation and Grad's moment method<sup>29</sup>.

Eu applied his theory to numerous practical applications for example, in the calculation of transport properties in gases<sup>30</sup>, in semiconductors<sup>31</sup>, Knudsen problem<sup>32</sup>, rigid diatomic gases<sup>33</sup>, sound waves absorption and dispersion<sup>34</sup> and found better applicability to situations far from equilibrium as compared to the Navier-Stokes-Fourier formulation. A high degree of non-equilibrium, as is observed in shock structures<sup>35</sup>, was studied using Eu's GH, and good agreements with experiments were observed at all Mach numbers.

Myong<sup>36</sup> modified the original generalized hydrodynamics formulation, leading to a simplified yet robust set of coupled algebraic equations for the non-conserved variables. The modified formulation was known as the nonlinear coupled constitutive relations (NCCR). The NCCR was proven

to be equivalent to the original formulation and was computationally less expensive. NCCR formulation was applied to study several non-equilibrium problems<sup>37,38</sup>. Myong<sup>4</sup> extended NCCR to diatomic gases by incorporating the bulk viscosity approach into the NCCR formulation. Recently, Yuan et al.<sup>39</sup> introduced a multi-temperature approach to study non-equilibrium phenomena in diatomic gases using a formulation similar to NCCR. They, however, kept bulk viscosity in their formulation along with the equation of excess stress.

The multi-temperature NCCR formulation was employed to study vibrational non-equilibrium by Mankodi et al.<sup>40</sup>. The rotational degree was assumed to be in equilibrium with the translational mode. Further, the NCCR formulation was extended to investigate the hypersonic reacting flows<sup>41</sup> with the vibrational degree of freedom<sup>42</sup>. It was found closer to the wind tunnel experiments, in-flight tests, and direct simulation Monte Carlo method than the NSF formulation.

A novel multi-temperature formulation was extended by Kumar et al.<sup>43</sup> where they considered the overall temperature and the dynamic temperature representing the internal degrees of freedom. A linear relationship was assumed between the translational and internal heat fluxes. The constitutive relations were obtained using an extended Gibbs relationship<sup>44</sup> and by enforcing the second law of inequality. A satisfactory match with the experimental and DSMC shock profiles was obtained up to Mach 10, compared to the NSF formulation, especially at Mach 6.1.

It is generally assumed that the rotational mode equilibrates very fast and can be taken as equal to the translational temperature leading to a two-temperature formulation<sup>45</sup>. However, the shock tube experiments, performed by Sharma et al.<sup>46</sup> and Fujita et al.<sup>47</sup> show that at high temperatures, the rate of rotational relaxation is slower. They found that the rotational temperature was closer to the vibrational temperature, unlike the two-temperature model where the rotational temperature is equal to the translational temperature. Further, the numerical studies performed by Furudate et al.<sup>48</sup> to calculate the shock standoff distance in a flow past sphere case, matched with the experiments when some finite rate rotational relaxation was accounted.

The present study incorporated the multi-temperature approach to diatomic gases to handle translational-rotational non-equilibrium within the NCCR framework for flow conditions far from equilibrium. Specifically, a shock structure study was chosen to investigate the high degree of non-equilibrium, observed at high Mach numbers. Despite the limitations of Parker's<sup>20</sup> model, it was employed in this study for simplicity. The present study aimed to investigate the role of higher-order constitutive theory in a multi-temperature framework. A comparison was made with the first-order Navier-Stokes-Fourier formulation, to determine the range of applicability of the

lower-order schemes, and then with experimental/DSMC data, to measure the accuracy of the new second-order constitutive relations.

This paper has been divided into sections, as follows. The derivation of the new set of governing equations related to NCCR formulation and the implementation of the multi-temperature approach are described in Section II. The section also includes relevant non-dimensionalization and the statements of various assumptions used to derive the NCCR equations. A short discussion on topological analysis for different combinations of non-conserved variables has been presented in Section III, where the non-linear and coupled nature of the higher-order moments in the current scheme will be evident. The details of the shock structure problem and the choice of the modeling parameters are discussed in Section IV along with the numerical detail of the computational scheme used in the present work. A thorough analysis of the shock structure results is presented in Section V, followed by conclusions in Section VI.

## II. GOVERNING EQUATIONS

The fundamental equations governing the conservation of mass, momentum, and total energy remain the same as in the Navier-Stokes-Fourier formulation. The rotational energy may change into translational energy and vice versa. Hence, an additional equation for rotational energy evolution is needed to account for the exchange of energy between the two modes within the limits of the conservation of the total energy of the flow. The set of partial differential equations for the conserved variables ( $\rho$ ,  $\rho\mathbf{u}$  and  $\rho E$ ) along with the energy equation for the rotational degree of freedom and the equation of state is as follows.

$$\frac{\partial \rho}{\partial t} + \nabla \cdot (\rho \mathbf{u}) = 0 \quad (4)$$

$$\frac{\partial}{\partial t}(\rho \mathbf{u}) + \nabla \cdot (p \mathbf{I} + \rho \mathbf{u} \mathbf{u}) + \nabla \cdot \mathbf{\Pi} = 0 \quad (5)$$

$$\frac{\partial}{\partial t}(\rho E) + \nabla \cdot [(\rho E + p) \mathbf{u}] + \nabla \cdot (\mathbf{\Pi} \cdot \mathbf{u} + \mathbf{Q}) = 0 \quad (6)$$

$$\frac{\partial}{\partial t}(\rho E_r) + \nabla \cdot [(\rho E_r) \mathbf{u}] + \nabla \cdot \mathbf{Q}_r = S_r \quad (7)$$

where  $E$  is the total energy per unit volume,  $E_r$  is the rotational energy per unit volume,  $\mathbf{Q}$  is the total heat flux ( $= \{\mathbf{Q}_t + \mathbf{Q}_r\}$ ), and  $\mathbf{Q}_r$  is the rotational heat flux. The total energy ( $E$ ), translational energy ( $E_t$ ), and rotational energy ( $E_r$ ) densities per unit volume are defined below.

$$E_r = RT_r \quad (8)$$

$$E_t = \frac{1}{2}u^2 + \frac{3}{2}RT_t \quad (9)$$

$$E = E_t + E_r \quad (10)$$

where  $T_t$  is the translational temperature and  $T_r$  is the rotational temperature. The closure is provided by the equation of state, as given below.

$$p = \rho RT_t \quad (11)$$

where  $R$  is the gas constant. The inter-mode energy exchange is accounted for by including a source term ( $S_r$ ) in the rotational energy evolution equation. The source term not only accounts for the amount of energy exchange but also the direction of relaxation depending on whether the flow is being compressed ( $E_t > E_r$ ) or expanded ( $E_r > E_t$ ).

The source term modeling is challenging as it involves the determination of complex inter-molecular energy exchanges. In the present derivation, the rotational-translational source term is modeled using the Landau-Teller-Jeans relaxation model, which is given as.

$$S_r = \frac{\rho R}{Z_r \tau_c} (T_t - T_r) \quad (12)$$

where  $Z_r$  is the rotational collision number and  $\tau_c$ , is the mean collision time, given through the following formulation:

$$\tau_c = \frac{\eta}{p} \quad (13)$$

where  $\eta$  represents the coefficient of shear viscosity. The dependence of rotational collision number ( $Z_r$ ) on translational temperature can be estimated using Parker's formulation<sup>20</sup> which has the following form<sup>21</sup>:

$$Z_r(T_t) = \frac{Z_r^\infty}{\left[ 1 + \frac{\pi^{\frac{3}{2}}}{2} \left( \frac{T'}{T_t} \right)^{\frac{1}{2}} + \left( 2 + \frac{\pi^2}{4} \right) \left( \frac{T'}{T_t} \right) \right]} \quad (14)$$

where  $T'$  and  $Z_r^\infty$  are gas specific parameters. The corresponding values for  $N_2$ ,  $O_2$  and  $Cl_2$  were provided by Parker<sup>20</sup>.

The higher-order non-conserved moments in the momentum and energy conservation equations will be calculated using the generalized hydrodynamics<sup>28</sup> approach. The equation for the evolution of any higher-order moment takes the following general form:

$$\rho \frac{d}{dt} \hat{\phi}^{(\alpha)} = Z^{(\alpha)} + \Lambda^{(\alpha)} \quad (15)$$

where  $\hat{\phi} = \phi/\rho$  denotes the intensive property of the higher-order moment  $\phi$ ,  $Z^{(\alpha)}$  is the kinematic term, and  $\Lambda^{(\alpha)}$  is the dissipative term<sup>28</sup>.

The evolution equation for stress can be obtained with  $\phi = \mathbf{\Pi}$  that can be simplified to the following form:

$$\rho \frac{d\hat{\mathbf{\Pi}}}{dt} = -\nabla \cdot \psi_2 - 2[\mathbf{\Pi} \cdot \nabla \mathbf{u}]^{(2)} - \frac{p}{\eta} \{ \mathbf{\Pi} q(\kappa) + 2\eta [\nabla \mathbf{u}]^{(2)} \} \quad (16)$$

where  $\psi_2$  is the higher order moment that should be evaluated and  $[\nabla \mathbf{u}]^{(2)} = \frac{1}{2}[\nabla \mathbf{u} + (\nabla \mathbf{u})^T] - \frac{1}{3}(\nabla \cdot \mathbf{u})\mathbf{I}$ . This forms a complete set of infinite evolution equations, as the evolution equation of each flux will have a higher-order moment in it. For practical limitations, a closure is needed to limit the evolution equations to some definite set.

Similarly, for translational heat flux,  $\phi = \mathbf{Q}_t$  is substituted which finally leads to:

$$\begin{aligned} \rho \frac{d\hat{\mathbf{Q}}_t}{dt} = & -\nabla \cdot \psi_3 + \nabla \cdot (p\mathbf{I} + \mathbf{\Pi}) \cdot \frac{\mathbf{\Pi}}{\rho} - \mathbf{Q}_t \cdot (\nabla \mathbf{u}) - \phi^{(3)} : (\nabla \mathbf{u}) \\ & - C_{p,t} \mathbf{\Pi} \cdot \nabla T_t - \frac{C_{p,t} p}{k_t} \left\{ k_t T_t \nabla (\ln T_t) + \mathbf{Q}_t q(\kappa) \right\} \end{aligned} \quad (17)$$

where  $k_t$  and  $C_{p,t}$  are the thermal conductivity and specific heat capacity at constant pressure corresponding to the translational mode, and  $\psi_3$  is the higher order flux. The evolution equation for translational heat flux is the same as that of total heat flux in the case of a monoatomic gas. This seems logical, as the monoatomic gas has only the translational degree of freedom. The  $C_{p,t}$  is taken as  $5/3R$ , the monoatomic equivalent value as the equation is assumed to be written for the translational degree of freedom only.

Similar to the translational heat flux equation, rotational heat flux will take a similar form with parameters corresponding to rotational energy. Since, the term  $\nabla \cdot (p\mathbf{I} + \mathbf{\Pi}) \cdot (\mathbf{\Pi}/\rho)$  depends solely on the translational mode, it is absent in the formulation of the rotational energy evolution equation. The  $C_{p,r}$  and  $C_{v,r}$ , both specific heat capacities, are taken as  $R$  for rotational energy.

$$\rho \frac{d\hat{\mathbf{Q}}_r}{dt} = -\nabla \cdot \psi_4 - \mathbf{Q}_r \cdot (\nabla \mathbf{u}) - C_{p,r} \mathbf{\Pi} \cdot \nabla T_r - \frac{C_{p,r} p}{k_r} \left\{ k_r T_r \nabla (\ln T_r) + \mathbf{Q}_r q(\kappa) \right\} \quad (18)$$

where  $k_r$  and  $C_{p,r}$  are the thermal conductivity and specific heat capacity respectively corresponding to the rotational mode. Again,  $\psi_4$  is the higher order moment associated with the rotational flux equation. Equations 16, 17 and 18 involve a non-linear parameter,  $q(\kappa)$ , which is common to all evolution equations and is defined as

$$q(\kappa) = \frac{\sinh(\kappa)}{\kappa} \quad (19)$$

where  $\kappa$  is given as

$$\kappa = \frac{(mk_B)^{1/4} T_t^{1/4}}{\sqrt{2d} p} \left[ \frac{\mathbf{\Pi} : \mathbf{\Pi}}{2\eta} + \frac{\mathbf{Q}_t \cdot \mathbf{Q}_t / T_t}{k_t} + \frac{\mathbf{Q}_r \cdot \mathbf{Q}_r / T_r}{k_r} \right]^{1/2} \quad (20)$$

The form of ‘ $\kappa$ ’ in the present set of equations is analogous to the Rayleigh-Onsager dissipation function derived for the monoatomic gas case. It was extended to include the term  $(\mathbf{Q}_r \cdot \mathbf{Q}_r) / (T_r k_r)$  that corresponds to the rotational degree of freedom.

### A. Adiabatic Approximation

Since, the scale at which non-conserved moments change is much smaller than the scale at which macroscopic properties change, these moments were assumed to have reached their steady state with the infinitesimal change in macroscopic properties involved in their calculation. Hence, the non-conserved moment equations can be solved as steady-state equations with constant values of macroscopic variables. This approximation is known as the adiabatic approximation<sup>36</sup>.

Further, the higher order moment terms in the stress and energy equations ( $\psi_2, \psi_3, \phi^{(3)}, \psi_4$ ) need to be closed. Among closure theories, we employ the ‘closing-last balanced closure,’ proposed by Myong in 2014<sup>49</sup>. Myong observed that the number of places to be closed is two (movement and interaction), rather than one (movement only). The order of approximations in handling the kinematic (movement)  $\psi$  and dissipation (interaction)  $\Lambda^{(\alpha)}$  terms must be the same to satisfy balancing, for instance, the second-order closure for both terms. The present balanced closure effectively resolves the weakness of Eu’s closure<sup>35</sup>, where it was assumed that  $\psi_\alpha = 0$ . This was challenged by mathematicians and physicists for its inconsistency, i.e., that the term  $\psi_\alpha$  cannot be zero in general, especially in strong thermal non-equilibrium<sup>3</sup>. Rather Myong assumes the following relations to be valid.

$$\nabla \cdot \psi_2 = \nabla \cdot \psi_3 + \phi^{(3)} : \nabla \mathbf{u} = 0 \quad (21)$$

In this balanced closure theory, third-order closure for  $\psi_2$  in the constitutive equation of stress term may not be essential; in fact, the unbalanced higher-order closure in the moment method may not provide improved solutions as promised, especially in the case of a high Mach number shock structure problem.

The higher-order term associated with the vibrational heat flux equation is handled ( $\nabla \cdot \psi_4 = 0$ ) in the same way. We finally obtain the following set of second-order approximate NCCR equations.

$$-(\mathbf{u} \cdot \nabla)\mathbf{\Pi} - \mathbf{\Pi}(\nabla \cdot \mathbf{u}) - 2[\mathbf{\Pi} \cdot \nabla \mathbf{u}]^{(2)} - \frac{P}{\eta}[\mathbf{\Pi}q(\kappa) + 2\eta\{\nabla \mathbf{u}\}^{(2)}] = 0 \quad (22)$$

$$\begin{aligned} & -(\mathbf{u} \cdot \nabla)\mathbf{Q}_t - \mathbf{Q}_t(\nabla \cdot \mathbf{u}) + \nabla \cdot (p\mathbf{I} + \mathbf{\Pi}) \cdot \frac{\mathbf{\Pi}}{\rho} - \mathbf{Q}_t \cdot (\nabla \mathbf{u}) \\ & - C_{p,t}\mathbf{\Pi} \cdot \nabla T_t - \frac{C_{p,t}P}{k_t} \left\{ k_t T_t \nabla(\ln T_t) + \mathbf{Q}_t q(\kappa) \right\} = 0 \end{aligned} \quad (23)$$

$$\begin{aligned} & -(\mathbf{u} \cdot \nabla)\mathbf{Q}_r - \mathbf{Q}_r(\nabla \cdot \mathbf{u}) - \mathbf{Q}_r \cdot (\nabla \mathbf{u}) - C_{p,r}\mathbf{\Pi} \cdot \nabla T_r \\ & - \frac{C_{p,r}P}{k_r} \left\{ k_r \nabla(\ln T_r) + \mathbf{Q}_r q(\kappa) \right\} = 0 \end{aligned} \quad (24)$$

It was noted in the past that Eu's canonical distribution function in the exponential form might have some difficulty when it is truncated to a finite number of terms. A numerical difficulty may arise when calculating the normalization factor associated with the canonical distribution function because the heat flux contribution containing the third-order term for the integrand may give rise to the divergence causing a problem. Eu showed, however, that this difficulty can be avoided if the set is truncated in such a way as to produce a truncated distribution function in the fourth-order for the integrand while ensuring convergence of the integral<sup>2</sup>.

## B. Non-Dimensionalization of multi-temperature NCCR

The multi-temperature NCCR relations were non-dimensionalized using relevant reference values of the properties.

$$\begin{aligned} \mathbf{x}^* &= \mathbf{x}/L, & \eta^* &= \eta/\eta_{ref}, & \mathbf{u}^* &= \mathbf{u}/u_{ref} \\ p^* &= p/p_{ref} & \rho^* &= \rho/\rho_{ref}, & E^* &= E^*/u_{ref}^2 \\ E_r^* &= E_r^*/u_{ref}^2, & T_{(t/r)}^* &= T_{(t/r)}/T_{ref}, & t^* &= 1/(L/u_{ref}), \end{aligned}$$

where  $\Delta T$  is the difference between the wall temperature and local temperature and  $L$  is the length scale. The conservation laws in their non-dimensional form are given below.

$$k_{(t/r)}^* = k_{(t/r)}/k_{(t/r)ref}, \quad C_{p(t/r)}^* = C_{p(t/r)}/C_{p(t/r)ref}$$

$$\mathbf{\Pi}^* = \mathbf{\Pi}/(\eta_e u_{ref}/L), \quad \mathbf{Q}_{(t/r)}^* = \mathbf{Q}_{(t/r)}/(\kappa_{(t/r)}\Delta T/L)$$

$$\frac{\partial}{\partial t^*}\rho^* + \mathbf{\nabla}^* \cdot (\rho^* \mathbf{u}^*) = 0 \quad (25)$$

$$\frac{\partial}{\partial t^*}(\rho^* \mathbf{u}^*) + \mathbf{\nabla}^* \cdot \left( \frac{1}{N_\delta Re} p^* \mathbf{I} + \rho^* \mathbf{u}^* \mathbf{u}^* \right) + \mathbf{\nabla}^* \cdot \left( \mathbf{\Pi}^* \frac{1}{Re} \right) = 0 \quad (26)$$

$$\frac{\partial}{\partial t^*}(\rho^* E^*) + \mathbf{\nabla}^* \cdot \left( \rho^* E^* + p^* \frac{1}{N_\delta Re} \right) \mathbf{u}^* +$$

$$\left\{ \frac{1}{Re} \right\} \mathbf{\nabla}^* \cdot \left\{ \mathbf{\Pi}^* \cdot \mathbf{u}^* + \left( \frac{\mathbf{Q}_r^*}{Ec_r Pr} + \frac{\mathbf{Q}_t^*}{Ec_t Pr} \right) \right\} = 0 \quad (27)$$

$$\frac{\partial}{\partial t^*}(\rho^* E_r^*) + \mathbf{\nabla}^* \cdot (\rho^* E_r^*) \mathbf{u}^* + \left\{ \frac{1}{Re} \right\} \mathbf{\nabla}^* \cdot \left( \frac{\mathbf{Q}_r^*}{Ec_r Pr} \right) = S_r^* \quad (28)$$

where the Reynolds number ( $Re$ ), Prandtl number ( $Pr$ ), Eckart number ( $Ec_{(t/r)}$ ), Mach number ( $M$ ) and other non-dimensional parameters are defined as

$$N_\delta = \frac{\eta_{ref} u_{ref}}{p_{ref} L}, \quad Re = \frac{\rho_{ref} u_{ref} L}{\eta_{ref}}, \quad \mathbf{\nabla}^* = \frac{\partial}{\partial \mathbf{x}^*}, \quad M = \frac{u_{ref}}{\sqrt{\gamma R T_{ref}}}$$

$$Ec_{(t/r)} = \frac{u_{ref}^2}{C_{p,(t/r)ref} \Delta T}, \quad Pr = \frac{C_{(p,t)ref} \eta_{ref}}{\kappa_{(t)ref}} = \frac{C_{(p,r)ref} \eta_{ref}}{\kappa_{(r)ref}}$$

The non-dimensionalized form of the source term is given below.

$$S_r^* = \frac{1}{\gamma M^2} \frac{\rho^* (T_t^* - T_r^*)}{Z_r \tau^*} \quad (29)$$

The Eqns. 22, 23 and 24 can be approximated further following Myong's approximation<sup>36</sup> for monoatomic gases which are assumed for the current case of diatomic gases. The final set of equations in non-dimensional form for stress tensor, translational, and rotational heat flux are given below.

$$-2[\mathbf{\Pi}^* \cdot \mathbf{\nabla}^* \mathbf{u}^*]^{(2)} - \frac{1}{N_\delta} \frac{p^*}{\eta^*} \{ \mathbf{\Pi}^* q(\kappa^* N_\delta) + 2\eta^* [\mathbf{\nabla}^* \mathbf{u}^*]^{(2)} \} = 0 \quad (30)$$

$$-Pr \mathbf{\Pi}^* \cdot \mathbf{\nabla}^* T_t^* - \frac{Pr}{N_\delta} \frac{p^*}{k_t^*} \{ k_t^* T_t^* \mathbf{\nabla}^* (\ln T_t^*) + \mathbf{Q}_t^* q(N_\delta \kappa^*) \} = 0 \quad (31)$$

$$-Pr \mathbf{\Pi}^* \cdot \mathbf{\nabla}^* T_r^* - \frac{Pr}{N_\delta} \frac{p^*}{k_r^*} [k_r^* T_r^* \mathbf{\nabla}^* (\ln T_r^*) + \mathbf{Q}_r^* q(N_\delta \kappa^*)] = 0 \quad (32)$$

The non-linear term  $\kappa$  is non-dimensionalized as given below.

$$\kappa = \left( \frac{(mk_B T_{ref})^{1/4}}{d_{ref} \sqrt{\eta_{ref}}} \right) \frac{T_t^{*1/4} N_\delta}{2d^* \sqrt{\eta^* p^*}} \left[ \mathbf{\Pi}^* : \mathbf{\Pi}^* + 2\varepsilon_t \frac{\eta^*}{k_t^* T_t^*} \mathbf{Q}_t^* \cdot \mathbf{Q}_t^* + 2\varepsilon_r \frac{\eta^*}{k_r^* T_r^*} \mathbf{Q}_r^* \cdot \mathbf{Q}_r^* \right]^{1/2} \quad (33)$$

where

$$\varepsilon_{(t/r)} = \frac{\Delta T k_{(t/r)ref} \Delta T}{(\eta_{ref} u_{ref}^2) T_{ref}} = \frac{1}{Ec_{(t/r)Pr} T_{ref} / \Delta T} \quad (34)$$

and  $m$  is the mass of a molecule,  $k_B$  is the Boltzmann constant, and  $d_{ref}$  is the reference diameter.

The viscosity formula for simple gas using power law molecular interaction is<sup>6</sup> given below.

$$\eta = \frac{5 \sqrt{\left( \frac{k_B m T_t}{\pi} \right) \left( \frac{1}{d^2} \right)}}{8 \Gamma \left( 4 - \frac{2}{v-1} \right) A_2(v)}, \quad d = \left( \frac{K}{2k_B T_t} \right)^{\frac{1}{v-1}} \quad (35)$$

$$\Rightarrow \eta \propto T_t^{\left( \frac{1}{2} + \frac{2}{v-1} \right)}, \quad d \propto T_t^{\left( \frac{1}{1-v} \right)}$$

where  $v$  is the exponent of the inverse power laws. Using the above relations for  $\eta$  and  $d$ , the expression  $\frac{T_t^{*1/4}}{d^* \sqrt{\eta^*}}$  evaluates to 1 and

$$\left( \frac{(mk_B T_{ref})^{1/4}}{d_{ref} \sqrt{\eta_{ref}}} \right) = \left[ 8 \frac{\sqrt{\pi}}{5} \Gamma \left( 4 - \frac{2}{v-1} \right) A_2(v) \right]^{1/2} \quad (36)$$

Myong<sup>36</sup> defined a parameter  $c$  as given below.

$$c = \frac{1}{2} \left[ 8 \frac{\sqrt{\pi}}{5} \Gamma \left( 4 - \frac{2}{v-1} \right) A_2(v) \right]^{1/2} \quad (37)$$

Using the above definition of  $c$ ,  $\kappa$  can be written as given below.

$$\kappa = N_\delta k^* = \frac{c N_\delta}{p^*} \left[ \mathbf{\Pi}^* : \mathbf{\Pi}^* + 2\varepsilon_t \frac{\eta^*}{k_t^* T_t^*} \mathbf{Q}_t^* \cdot \mathbf{Q}_t^* + 2\varepsilon_r \frac{\eta^*}{k_r^* T_r^*} \mathbf{Q}_r^* \cdot \mathbf{Q}_r^* \right]^{1/2} \quad (38)$$

The value of  $c$  depends on the exponent in the power law model of inter-molecular interaction. For several values, they are calculated and tabulated in Table I.

The Hard sphere model is obtained with  $v = \infty$ , Maxwell's model with  $v = 5$  and the Variable Hard Sphere (VHS) model with  $v = 9$ .

Thermal conductivities are defined using the same value of the Prandtl number ( $Pr$ ). The non-dimensional relations for thermal conductivities can be derived using the definition of  $Pr = (\eta C_{p(t/r)}) / (k_{(t/r)})$ . Heat capacities are assumed to be independent of temperature.

$$k_t^* = \eta^*, \quad k_r^* = \eta^* \quad (39)$$

TABLE I. Calculated values of  $c$ 

| $\nu$                | $s = \left(\frac{1}{2} + \frac{2}{\nu-1}\right) A_2$ | $\Gamma$                          | $c$     |
|----------------------|------------------------------------------------------|-----------------------------------|---------|
| 5                    | 1                                                    | $0.436 \Gamma(3.5) = 3.32335$     | 1.01356 |
| 7                    | 0.833                                                | $0.357 \Gamma(3.6667) = 4.01222$  | 1.00773 |
| 9                    | 0.75                                                 | $0.332 \Gamma(3.75) = 4.2299$     | 1.02034 |
| 11                   | 0.7                                                  | $0.319 \Gamma(3.8) = 4.69417$     | 1.02927 |
| 15                   | 0.643                                                | $0.309 \Gamma(3.85714) = 5.02913$ | 1.04965 |
| 21                   | 0.6                                                  | $0.307 \Gamma(3.9) = 5.29933$     | 1.07398 |
| 25                   | 0.583                                                | $0.306 \Gamma(3.91667) = 5.40909$ | 1.08328 |
| $\rightarrow \infty$ | 0.5                                                  | $0.333 \Gamma(4) = 6$             | 1.19019 |

The equation of state ( $p = \rho RT$ ) can be non-dimensionalized as given below. Since pressure is predominantly a phenomenon observed due to the translational motion of molecules, only reference to translational temperature was made in the equation of state.

$$p^* = \rho^* T_t^* \quad (40)$$

For the speed of sound  $a^2 = \gamma RT_t$ , we have

$$a^{*2} = T_t^*/M^2 \quad (41)$$

The energy term  $\rho E = \frac{1}{2}\rho u^2 + \frac{3}{2}\rho RT_t + \rho RT_r$  can be written in the non-dimensional form as given below.

$$\rho^* E^* = \frac{1}{2}\rho^* u^{*2} + \left(\frac{1}{N_\delta Re}\right) \left(\frac{3}{2}T_t^* + T_r^*\right) \quad (42)$$

The non-dimensional specific heat capacity,  $C_{p,(t/r)}^*$  is numerically equal to 1 since  $C_{p,(t/r)ref} = C_{p,(t/r)}$  as translational or rotational degrees of freedom are fully excited and hence independent of temperature. If only terms containing  $N_\delta^{-1}$  in Eqns. (30), (31) and (32) are considered, we have

$$\mathbf{\Pi}^* q(N_\delta \kappa^*) = -2\eta^* [\mathbf{\nabla}^* \mathbf{u}^*]^{(2)} = \mathbf{\Pi}_0^* \quad (43)$$

$$\mathbf{Q}_t^* q(N_\delta \kappa^*) = -k_t^* T_t^* \mathbf{\nabla}^* (\ln T_t^*) = \mathbf{Q}_{t0}^* \quad (44)$$

$$\mathbf{Q}_r^* q(N_\delta \kappa^*) = -k_r^* T_r^* \mathbf{\nabla}^* (\ln T_r^*) = \mathbf{Q}_{r0}^* \quad (45)$$

If the product of above definitions of  $\mathbf{\Pi}^*$ ,  $\mathbf{Q}_t^*$  and  $\mathbf{Q}_r^*$  is formed

$$[q(N_\delta \kappa^*)]^2 \left(\frac{c}{p^*}\right)^2 [\mathbf{\Pi}^* : \mathbf{\Pi}^* + \mathbf{Q}_t^* \cdot \mathbf{Q}_t^* / (T_t^* / 2\varepsilon_t) + \mathbf{Q}_r^* \cdot \mathbf{Q}_r^* / (T_r^* / 2\varepsilon_r)] =$$

$$\left(\frac{c}{p^*}\right)^2 [\mathbf{\Pi}_0^* : \mathbf{\Pi}_0^* + \mathbf{Q}_{t0}^* \cdot \mathbf{Q}_{t0}^* / (T_t^* / 2\varepsilon_t) + \mathbf{Q}_{r0}^* \cdot \mathbf{Q}_{r0}^* / (T_r^* / 2\varepsilon_r)] \quad (46)$$

$$\Rightarrow q[(N_\delta \kappa^*)] \kappa^* = \kappa_0^* \quad (47)$$

Multiplying  $N_\delta$  to Eqn. (47) and using Eqns. (43, 44, 45) we can obtain the non-linear fluxes in their simplest forms.

$$\mathbf{\Pi}^* = \frac{\sinh^{-1}(N_\delta \kappa_0^*)}{(N_\delta \kappa_0^*)} \mathbf{\Pi}_0^*, \quad \mathbf{Q}_{t/r}^* = \frac{\sinh^{-1}(N_\delta \kappa_0^*)}{(N_\delta \kappa_0^*)} \mathbf{Q}_{t_0/r_0}^* \quad (48)$$

The Eqns. 30, 31, 32 can be further simplified using Eqns. 43,44, 45.

$$-2N_\delta \frac{\eta^*}{p^*} [\mathbf{\Pi}^* \cdot \nabla^* \mathbf{u}^*]^{(2)} - \{\mathbf{\Pi}^* q(\kappa^* N_\delta) - \mathbf{\Pi}_0^*\} = 0 \quad (49)$$

$$\frac{N_\delta}{p^*} \mathbf{\Pi}^* \cdot \mathbf{Q}_{t0}^* - [\mathbf{Q}_t^* q(N_\delta \kappa^*) - \mathbf{Q}_{t0}^*] = 0 \quad (50)$$

$$\frac{N_\delta}{p^*} \mathbf{\Pi}^* \cdot \mathbf{Q}_{r0}^* - \{\mathbf{Q}_r^* q(N_\delta \kappa^*) - \mathbf{Q}_{r0}^*\} = 0 \quad (51)$$

where

$$\nabla^* \hat{\mathbf{u}}^* = -2N_\delta \frac{\eta^*}{p^*} \nabla^* \mathbf{u}^*, \quad \hat{\mathbf{\Pi}}^* = \frac{N_\delta}{p^*} \mathbf{\Pi}^* \quad (52)$$

$$\hat{\mathbf{Q}}_t^* = \frac{N_\delta}{p^*} \frac{\mathbf{Q}_t^*}{\sqrt{T_t^* / 2\varepsilon_t}}, \quad \hat{\mathbf{Q}}_r^* = \frac{N_\delta}{p^*} \frac{\mathbf{Q}_r^*}{\sqrt{T_r^* / 2\varepsilon_r}} \quad (53)$$

and

$$\kappa = c\hat{R}, \quad q(c\hat{R}) = \frac{\sinh(c\hat{R})}{c\hat{R}} \quad (54)$$

$$\text{if } \hat{R} = \left[ \hat{\mathbf{\Pi}}^* : \hat{\mathbf{\Pi}}^* + \hat{\mathbf{Q}}_t^* \cdot \hat{\mathbf{Q}}_t^* + \hat{\mathbf{Q}}_r^* \cdot \hat{\mathbf{Q}}_r^* \right]^{1/2} \quad (55)$$

The final non-dimensional form of the NCCR equations are

$$\hat{\mathbf{\Pi}}^* q(c\hat{R}) = \hat{\mathbf{\Pi}}_0^* + [\hat{\mathbf{\Pi}}^* \cdot \nabla^* \hat{\mathbf{u}}^*]^{(2)} \quad (56)$$

$$\hat{\mathbf{Q}}_t^* q(c\hat{R}) = \hat{\mathbf{Q}}_{t0}^* + \hat{\mathbf{\Pi}}^* \cdot \hat{\mathbf{Q}}_{t0}^* \quad (57)$$

$$\hat{\mathbf{Q}}_r^* q(c\hat{R}) = \hat{\mathbf{Q}}_{r0}^* + \hat{\mathbf{\Pi}}^* \cdot \hat{\mathbf{Q}}_{r0}^* \quad (58)$$

The above equations can be simplified further for one dimensional cases. (The superscript \* and the subscripts  $xx$  and  $x$  have been dropped for simplicity.)

$$\hat{\Pi}q(c\hat{R}) = \hat{\Pi}_0 + \hat{\Pi}\hat{\Pi}_0 \quad (59)$$

$$\hat{Q}_tq(c\hat{R}) = \hat{Q}_{t0} + \hat{\Pi}\hat{Q}_{t0} \quad (60)$$

$$\hat{Q}_r q(c\hat{R}) = \hat{Q}_{r0} + \hat{\Pi}\hat{Q}_{r0} \quad (61)$$

and

$$\hat{R} = \left[ \frac{3}{2}\hat{\Pi}^{*2} + \hat{Q}_t^{*2} + \hat{Q}_r^{*2} \right]^{1/2} \quad (62)$$

The set of Eqns. 59, 60 and 61 represent a system of non-linear algebraic equations. The non-linear dependence is evident as each of them contains  $q(c\hat{R})$  term which is defined using the sinh function. Solving the above set of equations will demonstrate the coupled nature of NCCR non-conserved moments. The next section presents various sets of graphs that were obtained by solving Eqns. 59, 60 and 61 iteratively.

### III. TOPOLOGICAL ANALYSIS

A topological analysis was carried out to reveal the non-linear behavior of the present NCCR formulation. Topology is a mathematical concept useful for describing the properties of a system that remains invariant under continuous transformations. The core idea is that knowledge of the object is independent of its spatial embedding. For example, Singh et al.<sup>50</sup> showed that in the case of velocity shear, the topology of their constitutive model is governed by a conic section, which is expressed as a second-degree polynomial equation in the phase space. This topology is always smooth, having derivatives of all orders everywhere in the conic section. This type of topology of conic sections has also been observed in other scientific fields, particularly in the elliptical, parabolic, and hyperbolic orbits of the planets and comets in the solar system, which are governed by Kepler's laws.

The NCCR non-conserved moments are calculated for a given set of NSF non-conserved values. The topological plots in Fig. 1 were obtained by solving the set of relations for the non-dimensional non-conserved moments using iterative schemes while keeping a fixed value of  $\hat{Q}_{r,0}$  as 0, 10 and 20 respectively. The plots show three-dimensional sections of the complete four-dimensional space

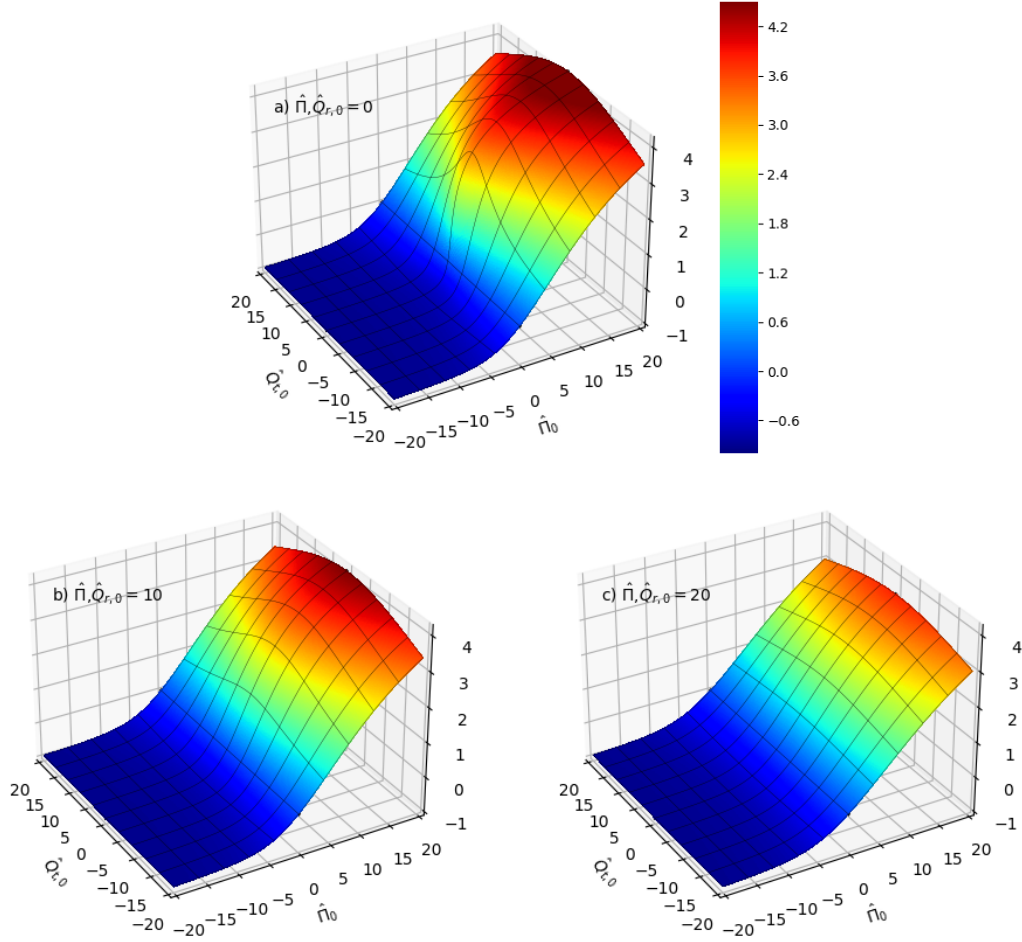


FIG. 1. Three-dimensional topology of NCCR  $\hat{\Pi}$  as a function of NSF  $\hat{\Pi}_0$  and NSF  $\hat{Q}_{t,0}$  at constant values of  $\hat{Q}_{r,0} =$  a) 0, b) 10 and c) 20 respectively

spanned by the non-conserved moments as four coordinates. The three coordinates are the first-order NSF formulation of  $\hat{Q}_{r,0}$ ,  $\hat{Q}_{t,0}$ ,  $\hat{\Pi}_0$  while the fourth is one among the three NCCR non-conserved moments.

The surface plots of non-dimensional NCCR stress ( $\hat{\Pi}$ ) shown in Fig. 1, follow the similar trend at various constant values of  $\hat{Q}_{r,0}$  with maximum NCCR  $\hat{\Pi}$  observed for the zero value of  $\hat{Q}_{r,0}$ . This maximum drops as the value of  $\hat{Q}_{r,0}$  increases. The plots are symmetric with respect to the  $\hat{Q}_{t,0} = 0$  plane, which signifies the polarity independence of  $\hat{\Pi}$  with  $\hat{Q}_{t,0}$ .  $\hat{\Pi}$  values however exhibit a significant increase as  $\hat{\Pi}_0$  changes its sign from -ve to +ve values, highlighting the non-linear asymmetrical nature of  $\hat{\Pi}$ .

The surface plots of NCCR translational heat flux ( $\hat{Q}_t$ ) shown in Fig. 2 depicts as rotational symmetry around the  $\hat{Q}_{t,0} = 0$  axis. Here, the straight grid line in the middle of the contour can

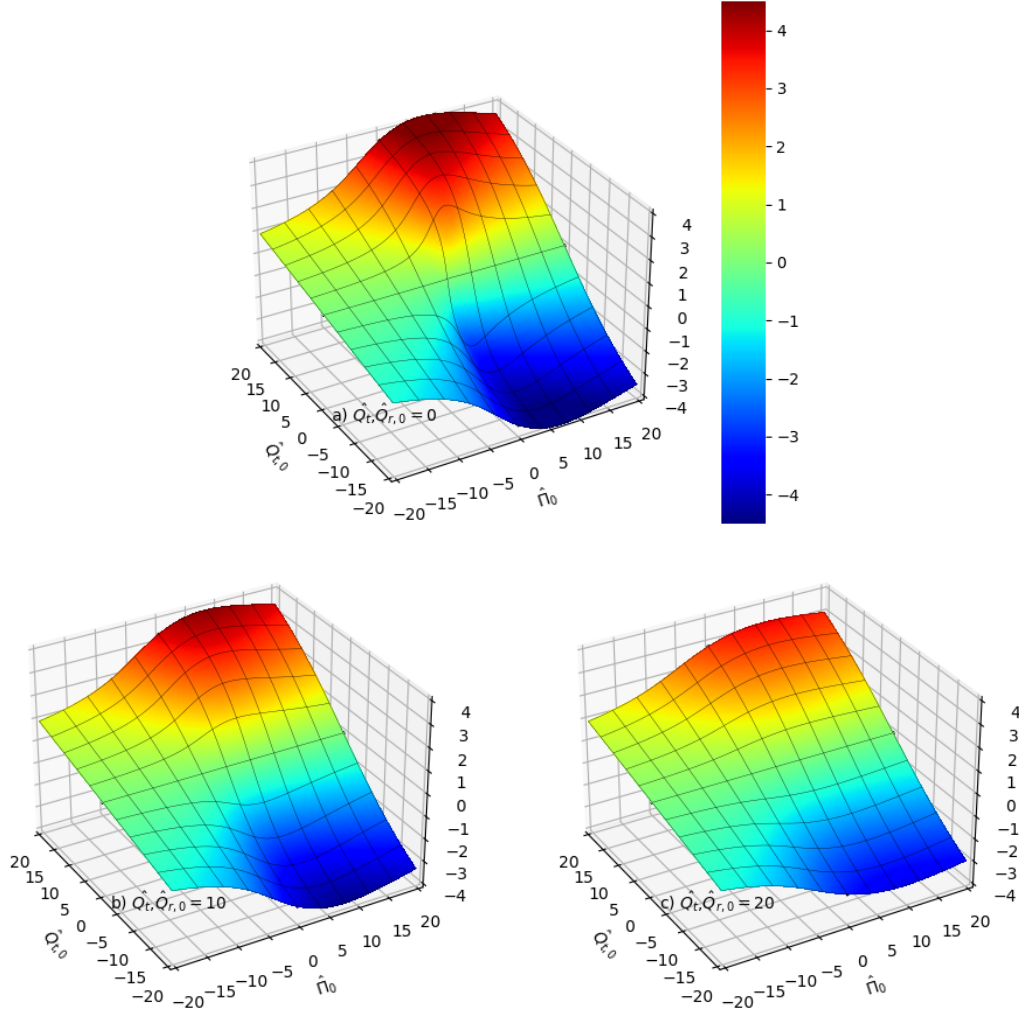


FIG. 2. Three-dimensional topology of NCCR  $\hat{Q}_t$  as a function of NSF  $\hat{\Pi}_0$  and NSF  $\hat{Q}_{t,0}$  at constant values of  $\hat{Q}_{r,0} =$  a) 0, b) 10 and c) 20 respectively

be regarded as the line of symmetry. The maximum and minimum values of  $\hat{Q}_t$  are the same in magnitude and are found when  $\hat{\Pi}_0$  is positive. Similar to the previous observation, the magnitude of both the extrema decreases as  $\hat{Q}_{r,0}$  increases from 0 to 20. The polarity of  $\hat{Q}_t$  depends on the polarity of  $\hat{Q}_{t,0}$ .

The variation in  $\hat{Q}_r$  with respect to  $\hat{Q}_{t,0}$  and  $\hat{\Pi}_0$  is shown in Fig. 3. For zero value of NSF  $\hat{Q}_{r,0}$ , the NCCR  $\hat{Q}_r$  is zero for any combinations of  $\hat{Q}_{t,0}$ , and  $\hat{\Pi}_0$  as shown in Fig. 3(a). For non-zero values of  $\hat{Q}_{r,0}$ , the plot is characterized with a dome containing the maximum  $\hat{Q}_r$  value. This maximum value increases with an increase in  $\hat{Q}_{r,0}$  value. The NCCR  $Q_r$  surface shifts upwards with an increase in the  $\hat{Q}_{r,0}$  value, as seen in Fig. 3(b) and (c).

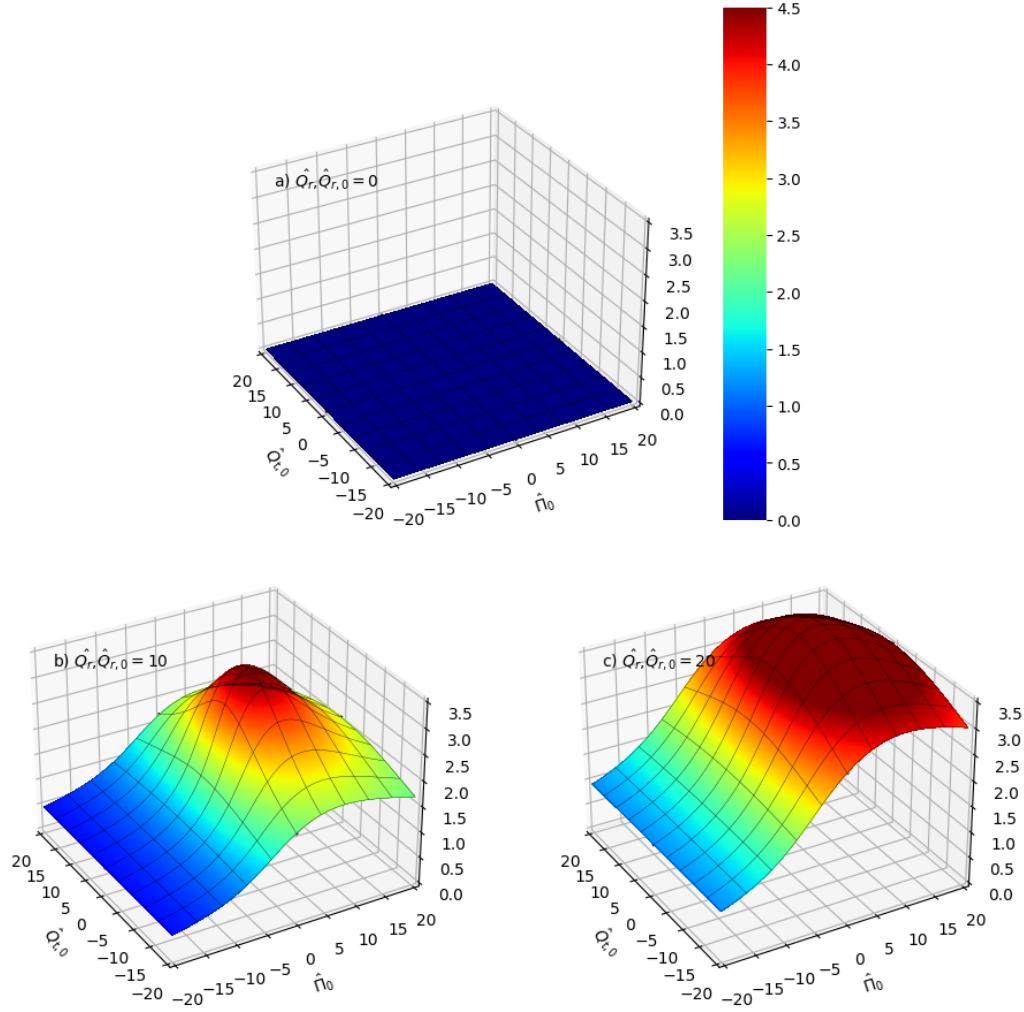


FIG. 3. Three-dimensional topology of NCCR  $\hat{Q}_r$  as a function of NSF  $\hat{\Pi}_0$  and NSF  $\hat{Q}_{t,0}$  at constant values of  $\hat{Q}_{r,0} =$  a) 0, b) 10 and c) 20 respectively

The NCCR translational heat flux ( $\hat{Q}_t$ ) as a function of NSF stress and rotational heat flux for a constant NSF translational heat flux is shown in Fig. 4. The topology is similar to that observed in Fig. 3(b). This is intuitive due to the similarity in the governing equations of translational and rotational heat fluxes.

Fig. 5 shows the plots of various NCCR non-conserved moments as a function of NSF  $\hat{Q}_{t,0}$  and NSF  $\hat{Q}_{r,0}$  for a constant value of NSF  $\hat{\Pi}_0$  equal to '10'. A prominent feature is the presence of a symmetric dome for the NCCR  $\hat{\Pi}$  observed in Fig. 5(a) which was found to increase as the value of  $\hat{\Pi}_0$  increases. The topologies of the NCCR translational and rotational heat flux (Fig. 5(b) and Fig. 5(c)) are equivalent, with the same maximum and minimum values.

The non-linear relationship between the NSF and NCCR fluxes provides some generalized pat-

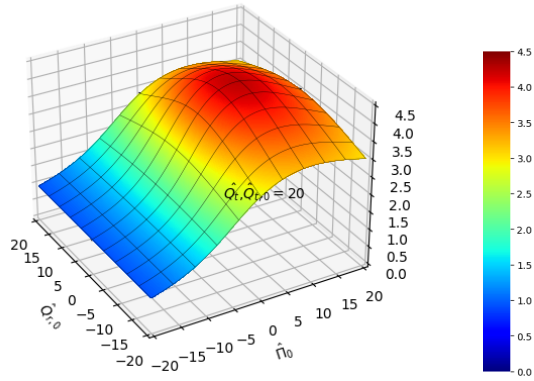


FIG. 4. Three-dimensional topology of NCCR  $\hat{Q}_t$  as a function of NSF  $\hat{\Pi}_0$  and NSF  $\hat{Q}_{r,0}$  at constant values of  $\hat{Q}_{t,0} = 20$  respectively

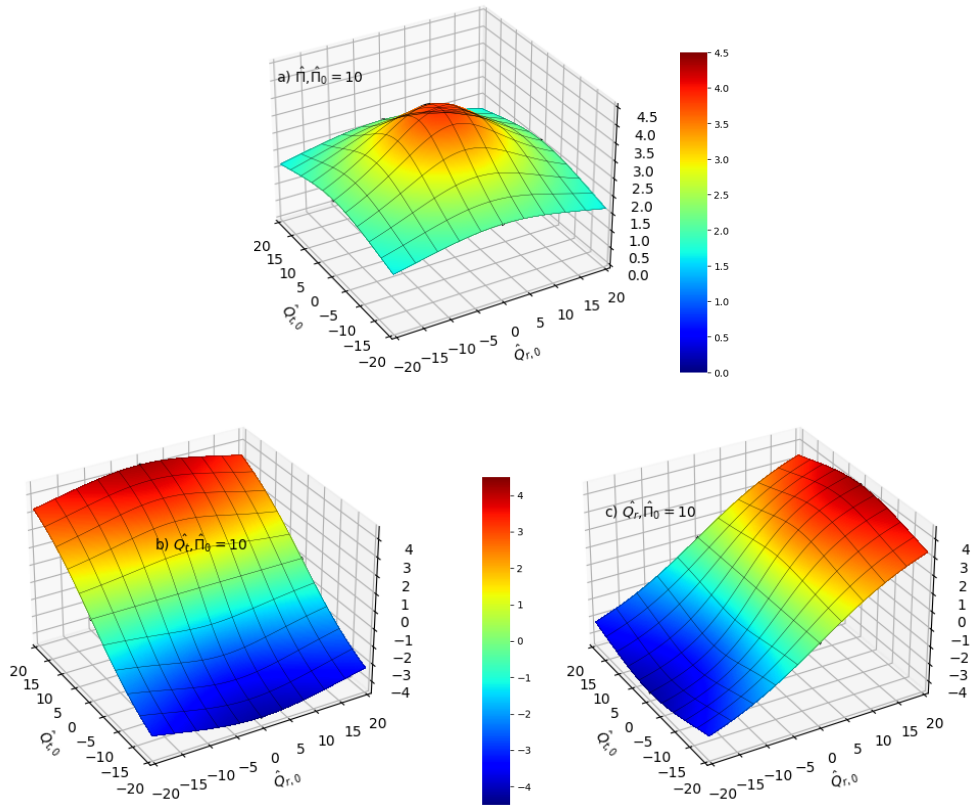


FIG. 5. Three-dimensional topology of NCCR non-conserved moments as a function of NSF  $\hat{Q}_{t,0}$  and NSF  $\hat{Q}_{r,0}$  at a constant value of  $\hat{\Pi}_0 = 10$

terms, observed as dome formation in the plots of  $\hat{Q}_r$  with constant values of  $\hat{Q}_{r,0}$ , the twisted contour plots for  $\hat{Q}_t$  with constant values of  $\hat{Q}_{r,0}$  and slide contour plots in  $\hat{\Pi}$  with constant values

of  $\hat{Q}_{r,0}$ . The similarity between the  $\hat{Q}_t$  and  $\hat{Q}_r$  fluxes can be concluded from Fig. 3 and Fig. 4 and from Fig. 5 (b) and 5 (c). Along the same line, the symmetric dome shape observed in Fig. 5 (a) shows the balanced dependency of NCCR stress  $\hat{\Pi}$ , over  $\hat{Q}_{t,0}$  and  $\hat{Q}_{r,0}$  fluxes.

#### IV. SHOCK STRUCTURE SIMULATIONS

Shock structure in a monoatomic gas was studied using the generalized hydrodynamics approach by Ghoul et al.<sup>35</sup>. Simplified viscosity models such as the power law model were used to compute the inverse density thickness ( $\delta^{-1}$ ) of shock structures over a range of Mach numbers. Inverse density thickness ( $\delta^{-1}$ ) is an intuitive measure of shock thickness. It is calculated using the maximum value of the slope in the density profile and is defined as:

$$\delta^{-1} = \frac{\left| \frac{\partial \rho}{\partial x} \right|_{max}}{\rho_2 - \rho_1} \quad (63)$$

where  $\rho_1$  and  $\rho_2$  are downstream and upstream values calculated using the Rankine-Hugoniot relations. Ghoul et al. found good agreements between the GH shock structure and experimental results<sup>35</sup>. The NCCR formulation was extended by Myong<sup>4</sup> to study shock waves in diatomic gases using the bulk viscosity approach. The results obtained through generalized hydrodynamics and NCCR were comparable to the experimental results at all Mach numbers. Shock structure was studied using multi-temperature NCCR formulation by Mankodi et al.<sup>40</sup> for Mach numbers ranging up to 15. A comparison between multi-temperature NSF, multi-temperature NCCR, and DSMC demonstrated the multi-temperature NCCR was more applicable as the degree of non-equilibrium increases with Mach number.

Shock structure involves a set of non-dimensional parameters that can be related to the Mach number of the flow. If the length scale  $L$  is taken equal to the mean free path based ( $\lambda$ ) on upstream conditions (reference conditions taken as the upstream values), we have the following relations between different non-dimensional parameters and Mach number.

$$Re = \sqrt{\frac{\gamma\pi}{2}} M_1, \quad N_\delta = M_1 \sqrt{\frac{2\gamma}{\pi}} \quad (64)$$

where  $\gamma$  is the ratio of heat capacities and  $M_1$  is the upstream Mach number. The mean free path of the flow in terms of upstream parameters (subscript '1') is given as:

$$\lambda = \sqrt{\frac{\pi}{2}} \frac{\eta_1}{\sqrt{RT_1} \rho_1} \quad (65)$$

For the shock structure analysis, the  $\Delta T$  in Eqn. 34 can be taken as  $T_{ref}$ , since there is no boundary temperature to compare with. The Eckart number  $Ec_{(t/r)}$  can be expressed as given below.

$$Ec_t = \frac{\gamma R}{C_{p,t1}} M_1^2 \quad \text{and} \quad Ec_r = \frac{\gamma R}{C_{p,r1}} M_1^2 \quad (66)$$

A separate Eckart number is defined for the translational and rotational modes since their specific heat capacities are different. The thermal conductivities are calculated using Eucken type relation.

$$k_{(t/r)} = \frac{\eta C_{p,(t/r)}}{Pr} \quad (67)$$

where the specific heat capacity at constant pressure for rotational and translational degrees are modeled as:

$$C_{p,t} = \frac{5}{2}R, \quad C_{p,r} = R \quad (68)$$

A one-dimensional domain spanning 60 times the mean free path (based on the driver-side parameters) and discretized using 500 grid points were used for the shock structure simulations. The advection upstream splitting method (AUSM) of Liou & Steffen<sup>51</sup> was implemented in the in-house finite volume method code to calculate the inviscid flux at control surfaces. Since higher gradients are involved, high-resolution schemes such as Monotonic Upstream-centered Scheme for Conservation Laws (MUSCL) - Hancock algorithm<sup>52</sup> were employed to obtain a better resolution. The viscous flux term is handled using the central difference scheme<sup>53</sup>. The NCCR formulation requires solving a system of non-linear equations, which were solved using iterative schemes. The properties of  $N_2$  gas were taken as standard temperature and pressure values of 273.15 K and, 101325 Pa, respectively. The  $Z_r^\infty$  value and other parameters for  $N_2$  gas are given in Table II.

For the conditions mentioned in Valentini et al.<sup>24</sup>, the nitrogen properties were the same as those given in Table II. However, the viscosity was modified and predicted using a power law for such low-temperature applications. The time step in the simulation is of the order of  $10^{-8}$  to  $10^{-10}$ . Grid-independent tests were performed up to a grid size of 1000, however no appreciable change was observed.

TABLE II. Properties of nitrogen

|                           |                       |
|---------------------------|-----------------------|
| Gas                       | $N_2$                 |
| R ( $J/kgK$ )             | 296.72                |
| Pr                        | 0.72                  |
| $\eta_{ref}$ ( $Ns/m^2$ ) | $1.66 \times 10^{-5}$ |
| $Z_r^\infty$              | 15.7                  |
| $T'$ (K)                  | 80                    |

## V. RESULTS AND DISCUSSION

Primitive variables such as density, pressure, temperature, and velocity were normalized using their upstream ( $X_1$ ) and downstream ( $X_2$ ) values. The generic form is given below.

$$X^* = \frac{X - X_1}{|X_2 - X_1|} \quad (69)$$

Since velocity decreases in the shock region, it would be more intuitive if it is normalized using  $X - X_2$  in the numerator.

Valentini et al.<sup>24</sup> carried out MD simulations at two sets of conditions and compared their results with experiments. The parameters they considered for their study were.

- $M_1 = 7.0$ .  $T_1 = 28.3$  K ( $\rho_1 = 0.1$  kg/m<sup>3</sup>)
- $M_1 = 12.7$ .  $T_1 = 9.0$  K ( $\rho_1 = 0.05$  kg/m<sup>3</sup>)

It can be seen that the temperatures considered by Valentini et al.<sup>24</sup> are very close to the characteristic rotational temperature, which for the  $N_2$  gas is 2.9 K. The above conditions correspond to pressures of 839.7176 Pa for the Mach 7 case and 133.524 Pa for the Mach 12.7 case respectively. The post-shock temperatures are well below the characteristic vibrational temperatures.

To test the validity of the present approach, the two-temperature NCCR formulation was applied to simulate the shock structure at the conditions studied by Valentini et al.<sup>24</sup>. Substantial improvements over the NSF formulation were observed in the upstream section while marginal improvements were found in the downstream section of the shock structure, as evident from the normalized density and temperature variations shown in Fig. 6 and Fig. 7, respectively, at Mach

7. Similar observations in density as well as rotational temperature profiles at Mach 12.7 were found, as shown in Fig. 8 and Fig. 9. It is noteworthy that the NCCR profiles are very close to the experimental and molecular dynamics data, especially in the upstream region.

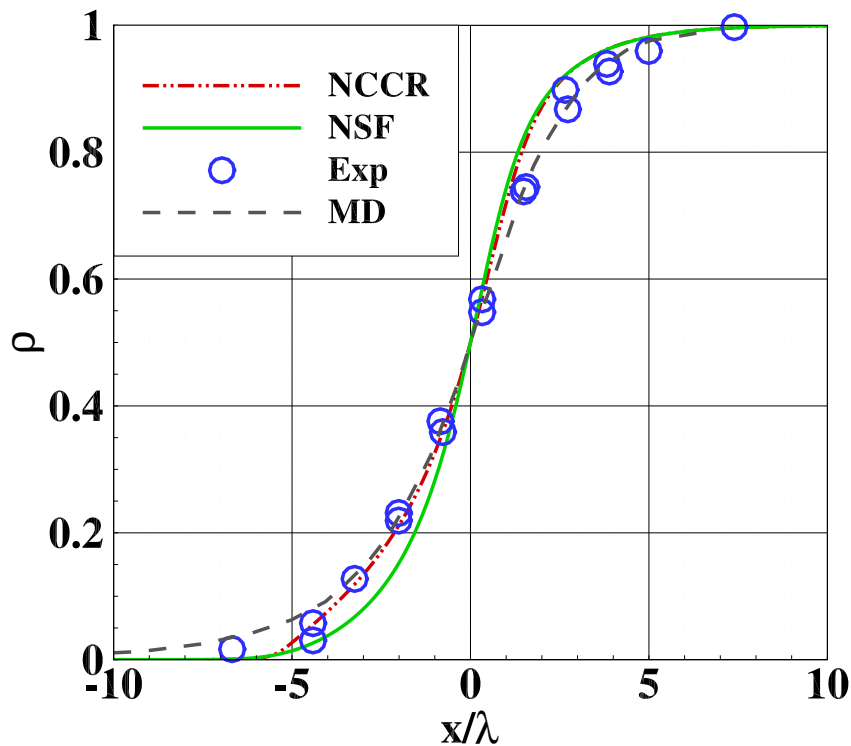


FIG. 6. Density profile comparison between Experiment, MD, NSF and NCCR formulations at Mach 7.

Apart from the approximations inherent in the generalized hydrodynamics approach followed in this study, the mismatch observed in the downstream section can be attributed to several other reasons. The Power law viscosity model, employed here, is an extremely simple model and may not be a good representation of inter-molecular forces at the low temperatures captured by experiments. Moreover, Parker's model is a classical model and ignores the quantum effects completely, which may be significant at such low temperatures. Moreover, the differences observed in the experimental and DSMC and MD results can be attributed to quantum effects, which were neglected in such simulations.

To circumvent such complications at extremely low temperatures and pressures, another set of simulations was performed at the STP conditions, and the shock structure profiles were compared

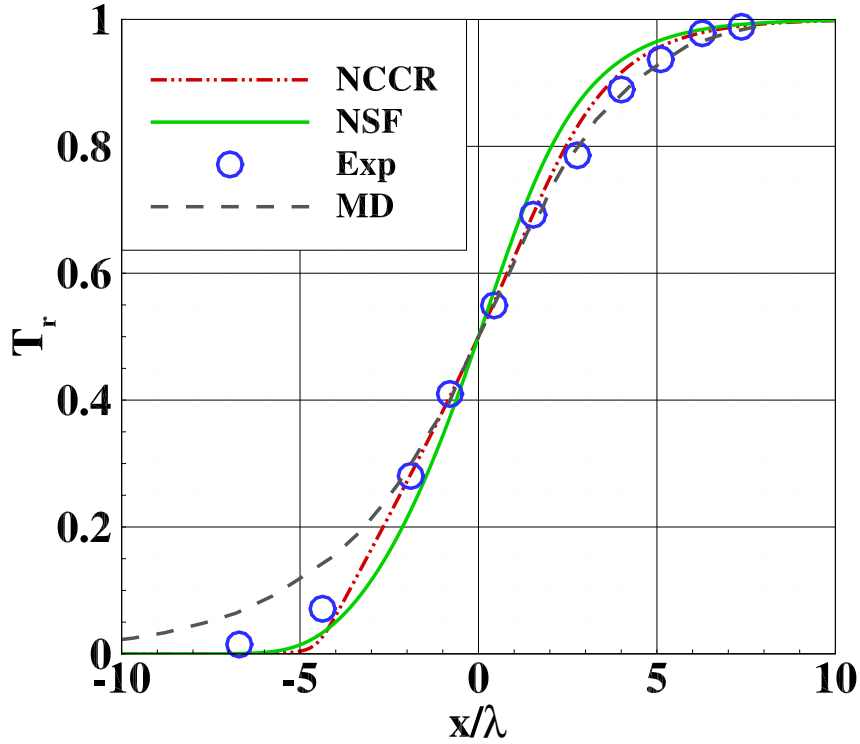


FIG. 7. Comparison of rotational temperature profiles from Experiment, MD, NSF and NCCR formulations at Mach 7.

with those obtained using the DSMC method<sup>39</sup>. Fig. 10 shows such a comparison at Mach 5. The conditions at the driver and driven side are listed in Table III.

TABLE III. Property values at Mach 5

|                 | Driver   | Driven    |
|-----------------|----------|-----------|
| Pressure (Pa)   | 101325.0 | 2938424.9 |
| Temperature (K) | 273.149  | 1584.269  |
| Mach            | 5.0      | 0.415     |

From Table III, we find that the post-shock temperature is well below the characteristic temperature for vibrational excitation, which for common gases such as  $N_2$  and  $O_2$  are 3390 K and 2270 K respectively. However, the involvement of vibrational degrees of freedom may become important as the Mach number increases as the post-shock temperature at Mach 10 was around,

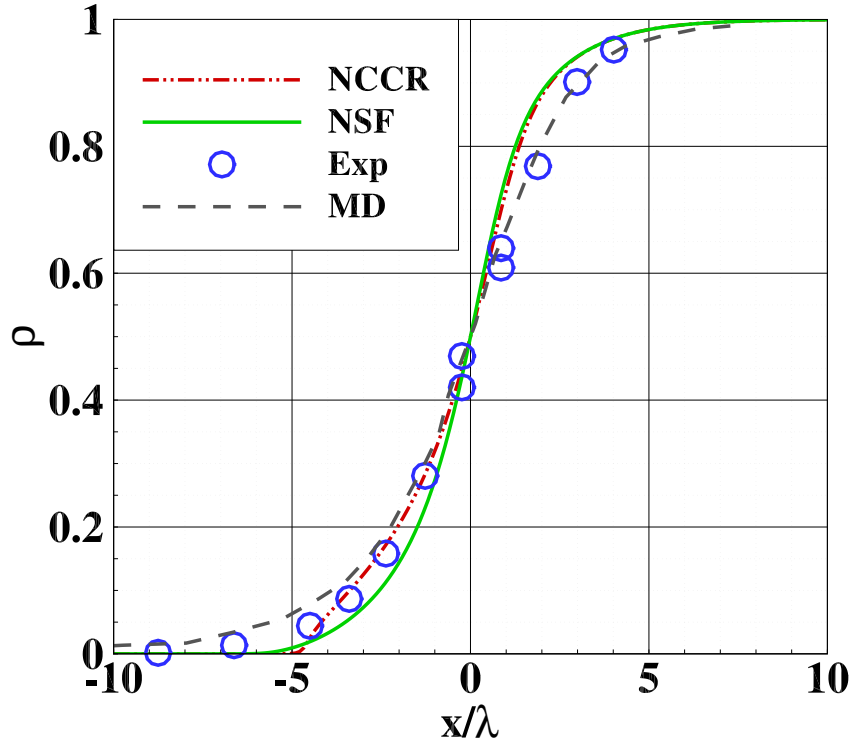


FIG. 8. Comparison of density profiles from Experiment, MD, NSF, and NCCR formulations at Mach 12.7.

5569 K. Nevertheless, in the present work, the vibrational degrees were neglected to keep the analysis simple. However, a more accurate study should involve three temperatures to characterize the three different degrees of freedom.

The density profile obtained using NCCR perfectly matches the upstream regions of the DSMC results. Non-dimensional translational and rotational temperature profiles are shown in Fig. 11 to show the degree of non-equilibrium between the rotational and translational modes of energy. Compared to the shock structure profiles obtained using the NSF, the NCCR profiles better match the shock structure profile obtained using the DSMC results at Mach 5. The relative position of both profiles is also comparable to that of the DSMC. The peak translational temperature achieved in DSMC was comparable to the NCCR and NSF formulations.

Figure 12 shows the density profiles obtained through multi-temperature NSF and NCCR, in comparison to the DSMC data at Mach 10. The smooth transition observed in the DSMC data near the upstream section is effectively captured with the multi-temperature NCCR. The multi-

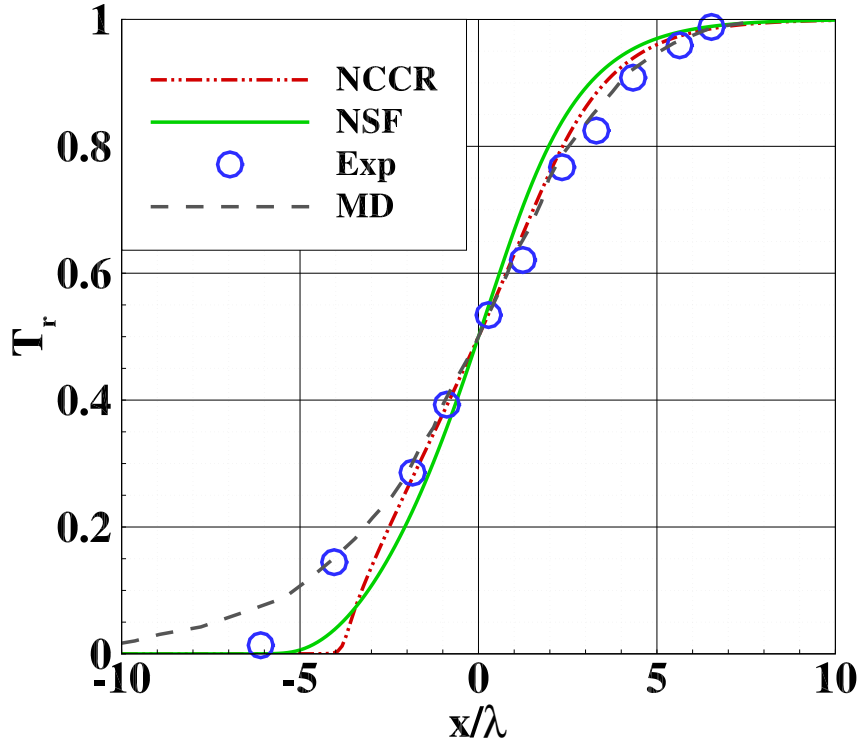


FIG. 9. Comparison of rotational temperature profiles from Experiment, MD, NSF, and NCCR formulations at Mach 12.7.

temperature NSF offers a smooth transition in the upstream region, however, the transition starts well after the DSMC transition.

A comparison between translational and rotational temperature profiles is shown in Fig. 13. Both multi-temperature NCCR and NSF lag behind the DSMC data. The multi-temperature NCCR translational temperature profile bulges out in the middle and runs closely to the DSMC translational temperature data. The rotational temperature profile from the multi-temperature NCCR is closer to that of the DSMC, especially in the upstream region. Moreover, the peak value of translational temperature in the DSMC simulation is higher than in the NCCR and NSF formulations. It should be noted that the effect of the vibrational degree of freedom will be significant, and it is expected that a three-temperature formulation may increase the accuracy of the current result.

Figure 14 compares the inverse density thickness profiles obtained using different formulations with the profile obtained using experiments<sup>18,54</sup>. The NSF multi-temperature (NSF [MT]) formu-

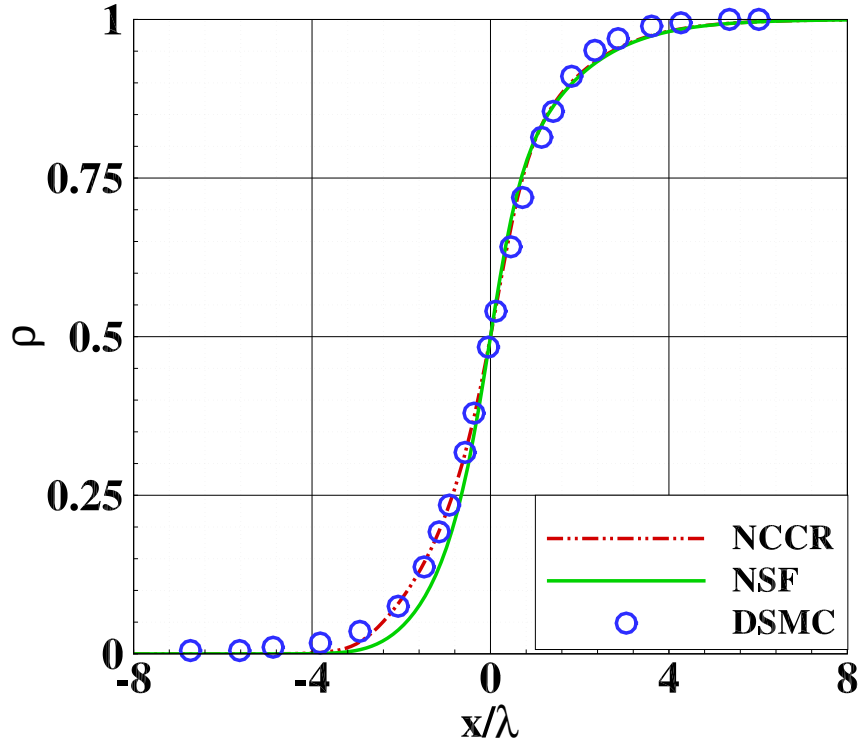


FIG. 10. Comparison of density profile profiles from NCCR, NSF, and DSMC at Mach 5

lation profile overestimates the experimental values at all Mach numbers. This trend is similar to that observed in the monoatomic gas case<sup>36</sup>. The NSF formulation calculates sharper density profiles due to the underestimation of fluxes at all Mach numbers. The NCCR bulk viscosity approach (NCCR [BV]) shown in Fig. 14 deviates from the experimental values beyond Mach 5. It is however closer to the experimental value at lower Mach numbers. Since the degree of non-equilibrium is not very high at lower Mach numbers, it is expected to provide good approximations.

The inverse density ( $\delta^{-1}$ ) profiles calculated using the multi-temperature NCCR formulation (NCCR [MT]) follow the general trend found in the experimental values. The profile seems to be shifted by a definite value. Still, there was a better match with the experimental scatter plot at hypersonic velocities. For lower Mach numbers, the multi-temperature formulation should predict results similar to those obtained using the bulk viscosity approach. However, the observed mismatch may be attributed to simplified  $Z_r$  models. It is expected that a better match may be observed when a more accurate model is used for the  $Z_r$  calculation. Nevertheless, the formulation

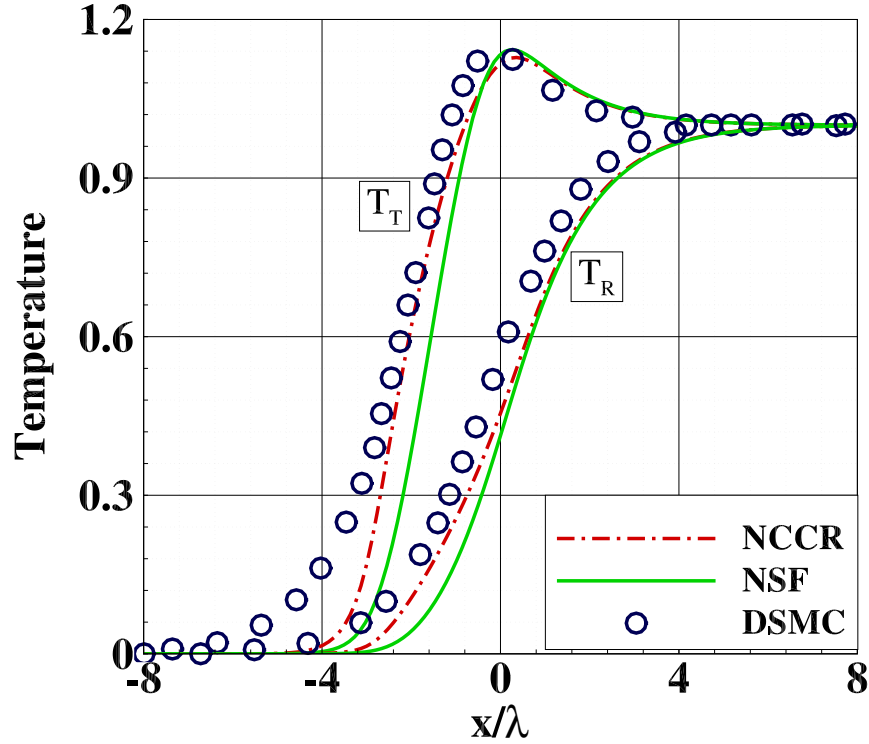


FIG. 11. Comparison of temperature profiles from NCCR, NSF, and DSMC at Mach 5

was closer to the experimental values at all Mach numbers compared with the multi-temperature NSF formulation.

Since the source term in the rotational energy evolution equation is a function of  $Z_r$ , its accurate estimation is of utmost importance when predicting various profiles. The present study utilizes Parker's model, which is a highly simplified classical approach to inter-molecular energy transfers.  $Z_r$  is a function of translational temperature, and Parker's model provides the explicit analytical expression for its calculation. However, a better match with experimental results can be obtained if  $Z_r$  is taken as a constant value for all Mach numbers. This observation is common to both the multi-temperature NSF as well as NCCR formulations. Constant shifts in  $\delta^{-1}$  profiles can be obtained when some suitable value of  $Z_r$  is taken. However, assuming a constant  $Z_r$  is counter-intuitive. Accordingly, this underlines the need to find more realistic  $Z_r$  models to accurately predict highly non-equilibrium phenomena.

## VI. CONCLUSIONS

Non-equilibrium thermodynamics involves complex phenomena, because of the involvement of conserved and non-conserved moments working at different scales. The calculation of these non-conserved moments becomes important as the degree of non-equilibrium increases. Since lower-order approximations such as NSF formulation fail to model these non-conserved moments accurately, especially when the degree of non-equilibrium is high, higher-order approximations should be employed to provide better predictions of non-equilibrium phenomena.

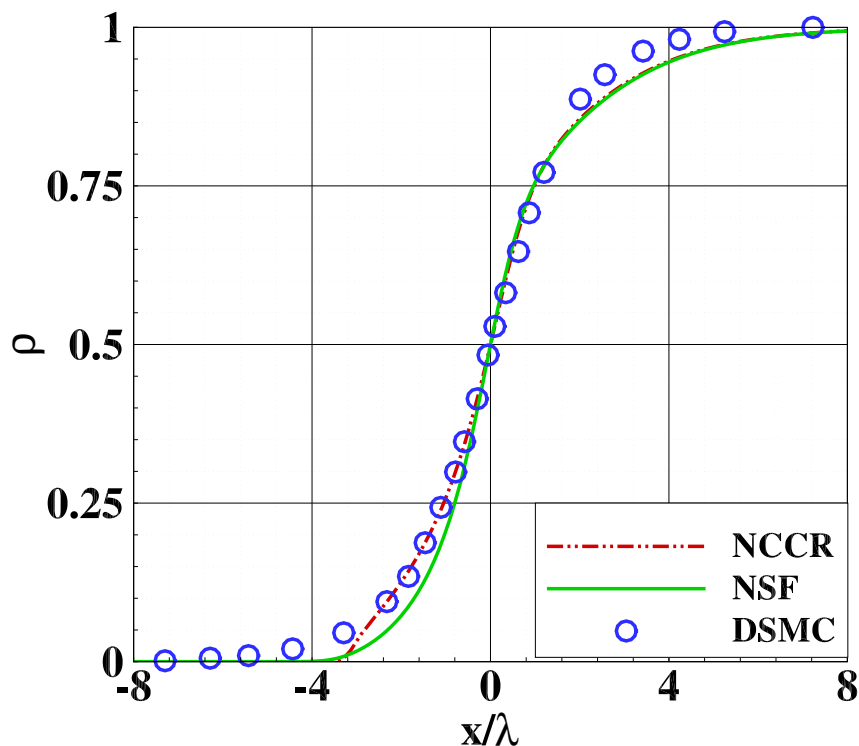


FIG. 12. Comparison of density profiles from NCCR, NSF, and DSMC at Mach 10

In this work, we derived and implemented the multi-temperature NCCR formulation for gas flows with rotational-translational non-equilibrium as an alternative to the bulk viscosity approach for gas flows with internal energy. The present formulation is computationally less expensive, compared to computationally expensive methods such as the DSMC and the MD methods. However, it produces much better results than NSF formulations, compared to those obtained using DSMC/MD simulations.

The new two-temperature NCCR formulation for diatomic gases was compared with the bulk viscosity approach and found to be better than the two-temperature NSF. Here, we extended its range of applications by introducing the rotational energy evolution equation, which accounts for rotational energy exchanges. The resultant formulation proved to be better at all values of Mach numbers when compared with the NSF formulation. A topological analysis was also carried out to demonstrate the nonlinearity present in the current formulation.

However, the limitations of the simplified phenomenological relaxation number-based rotational collision model cannot be overlooked. With improved collision models and better rotational collision calculations, we may expect the formulation to provide a better match with experimental results and DSMC/MD simulations at all Mach numbers.

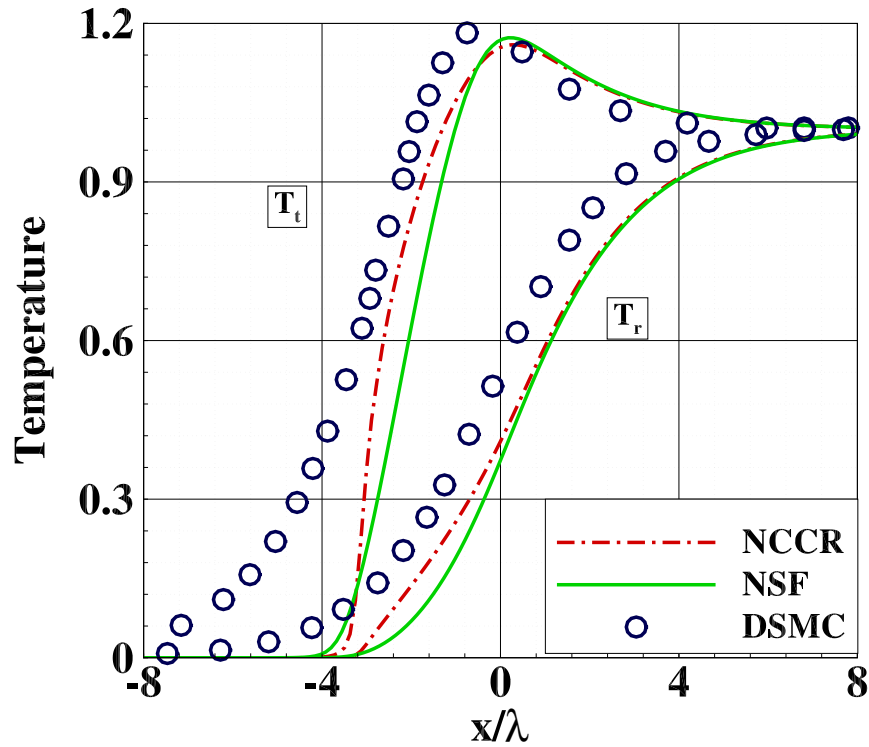


FIG. 13. Comparison of temperature profiles from NCCR, NSF, and DSMC at Mach 10

As mentioned in the previous section, the role of the vibrational degree of freedom becomes more significant when the Mach number of the flow is increased beyond a certain value. A three-temperature model to include the effect of vibrational degree of freedom along with rotational

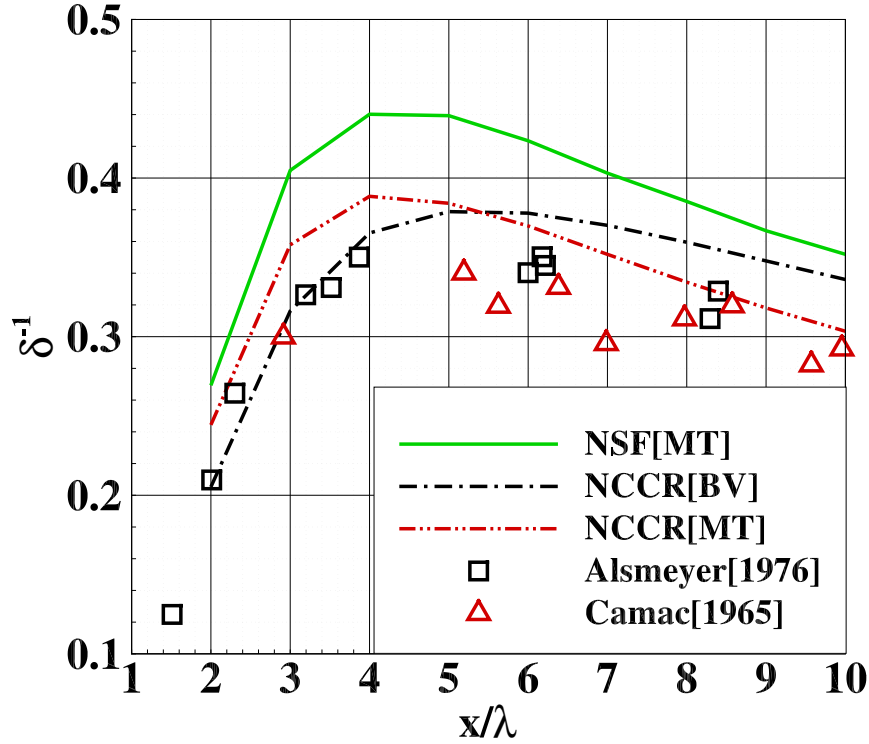


FIG. 14. Inverse Density thickness comparison

and translational degrees is expected to provide a more realistic picture of the non-equilibrium phenomena at high Mach numbers. Presently, an extension to multi-species is in progress as most of the high Mach flow applications will involve air as the common medium.

Multi-species will offer new challenges because of the presence of interspecies molecular collisions. Since the transport coefficients depend highly on the nature of the collisions, they should be modeled accordingly. Species diffusion and the assumption of common temperature for both species are some other factors that should be taken into consideration.

## ACKNOWLEDGEMENT

R.S.M was supported by the National Research Foundation of Korea (NRF) Grant funded by the Ministry of Science and ICT (RS-2024-00397400) and the Korea AeroSpace Administration (RS-2022-NR067079, Future Space Education Center), South Korea.

## CONFLICT OF INTEREST

The authors have no conflicts to disclose.

## DATA AVAILABILITY

The data that support the findings of this study are available from the corresponding authors upon request.

## REFERENCES

- <sup>1</sup>F. R. W. McCourt, J. J. M. Beenakker, W. E. Köhler, and I. Kuscer, *Nonequilibrium Phenomena in Polyatomic Gases* (Clarendon Press, Oxford, 1990) p. 276.
- <sup>2</sup>O. Ejtehadi, T. K. Mankodi, I. Sohn, B. J. Kim, and R. S. Myong, “Gas-particle flows in a microscale shock tube and collection efficiency in the jet impingement on a permeable surface,” *Physics of Fluids* **35**, 103324 (2023), <https://doi.org/10.1063/5.0170871>.
- <sup>3</sup>T. K. Mankodi, O. Ejtehadi, T. Chourushi, A. Rahimi, and R. S. Myong, “nccrFOAM suite: Nonlinear coupled constitutive relation solver in the OpenFOAM framework for rarefied and microscale gas flows with vibrational non-equilibrium,” *Computer Physics Communications* **296**, 109024 (2024), <https://doi.org/10.1016/j.cpc.2023.109024>.
- <sup>4</sup>R. S. Myong, “A generalized hydrodynamic computational model for rarefied and microscale diatomic gas flows,” *Journal of Computational Physics* **195**, 655–676 (2004), <https://doi.org/10.1016/j.jcp.2003.10.015>.
- <sup>5</sup>C. Curtiss, “Kinetic theory of nonspherical molecules,” *The Journal of Chemical Physics* **24**, 225–241 (1956), <https://doi.org/10.1063/1.1742459>.
- <sup>6</sup>S. Chapman and T. G. Cowling, *The Mathematical Theory of Non-Uniform Gases—An Account of the Kinetic Theory of Viscosity, Thermal Conduction and Diffusion in Gases* (Cambridge University Press, Cambridge, 1990).
- <sup>7</sup>C. S. Wang-Chang and G. E. Uhlenbeck, “Transport phenomenon in polyatomic gases,” *Tech. Rep. (Engineering Research Institute, University of Michigan, Ann Arbor, Report No. CM-681, 1951)*.
- <sup>8</sup>T. Morse, “Kinetic model for gases with internal degrees of freedom,” *Physics of Fluids* **7**, 159–169 (1964), <https://doi.org/10.1063/1.1711128>.

- <sup>9</sup>L. H. Holway, “New statistical models for kinetic theory: methods of construction,” *Physics of Fluids* **9**, 1658–1673 (1966), <https://doi.org/10.1063/1.1761920>.
- <sup>10</sup>Y. Dauvois, J. Mathiaud, and L. Mieussens, “An ES-BGK model for polyatomic gases in rotational and vibrational nonequilibrium,” *European Journal of Mechanics-B/Fluids* **88**, 1–16 (2021), <https://doi.org/10.1016/j.euromechflu.2021.02.006>.
- <sup>11</sup>V. Rykov, “A model kinetic equation for a gas with rotational degrees of freedom,” *Fluid Dynamics* **10**, 959–966 (1975), <https://doi.org/10.1007/BF01023275>.
- <sup>12</sup>V. Rykov, V. Titarev, and E. Shakhov, “Shock wave structure in a diatomic gas based on a kinetic model,” *Fluid Dynamics* **43**, 316–326 (2008), <https://doi.org/10.1134/S0015462808020178>.
- <sup>13</sup>I. N. Larina and V. A. Rykov, “Kinetic model of the Boltzmann equation for a diatomic gas with rotational degrees of freedom,” *Computational Mathematics and Mathematical Physics* **50**, 2118–2130 (2010), <https://doi.org/10.1134/S0965542510120134>.
- <sup>14</sup>C. Curtiss, “The classical Boltzmann equation of a gas of diatomic molecules,” *The Journal of Chemical Physics* **75**, 376–378 (1981), <https://doi.org/10.1063/1.441792>.
- <sup>15</sup>C. Curtiss, “The classical Boltzmann equation of a molecular gas,” *The Journal of Chemical Physics* **97**, 1416–1419 (1992), <https://doi.org/10.1063/1.463267>.
- <sup>16</sup>L. Wu, C. White, T. J. Scanlon, J. M. Reese, and Y. Zhang, “A kinetic model of the Boltzmann equation for non-vibrating polyatomic gases,” *Journal of Fluid Mechanics* **763**, 24–50 (2015), <https://doi.org/10.1017/jfm.2014.632>.
- <sup>17</sup>G. A. Bird, “Proceedings of 7th International Symposium on Rarefied Gas Dynamics,” **2**, 693 (1971).
- <sup>18</sup>H. Alsmeyer, “Density profiles in argon and nitrogen shock waves measured by the absorption of an electron beam,” *Journal of Fluid Mechanics* **74**, 497–513 (1976), <https://doi.org/10.1017/S0022112076001912>.
- <sup>19</sup>M. Linzer and D. Hornig, “Structure of shock fronts in argon and nitrogen,” *Physics of Fluids* **6**, 1661–1668 (1963), <https://doi.org/10.1063/1.1711007>.
- <sup>20</sup>J. Parker, “Rotational and vibrational relaxation in diatomic gases,” *Physics of Fluids* **2**, 449–462 (1959), <https://doi.org/10.1063/1.1724417>.
- <sup>21</sup>C. Brau and R. Jonkman, “Classical theory of rotational relaxation in diatomic gases,” *The Journal of Chemical Physics* **52**, 477–484 (1970), <https://doi.org/10.1063/1.1673010>.
- <sup>22</sup>E. Carnevale, C. Carey, and G. Larson, “Ultrasonic determination of rotational collision numbers and vibrational relaxation times of polyatomic gases at high temperatures,” *The Journal of*

- Chemical Physics **47**, 2829–2835 (1967), <https://doi.org/10.1063/1.1712305>.
- <sup>23</sup>C. Nyeland, “Rotational relaxation of homonuclear diatomic molecules,” The Journal of Chemical Physics **46**, 63–67 (1967), <https://doi.org/10.1063/1.1840430>.
- <sup>24</sup>P. Valentini, C. Zhang, and T. E. Schwartzentruber, “Molecular dynamics simulation of rotational relaxation in nitrogen: Implications for rotational collision number models,” Physics of Fluids **24**, 106101 (2012), <https://doi.org/10.1063/1.4757119>.
- <sup>25</sup>B. C. Eu, “A modified moment method and irreversible thermodynamics,” The Journal of Chemical Physics **73**, 2958–2969 (1980), <https://doi.org/10.1063/1.440469>.
- <sup>26</sup>H. Grad, “The profile of a steady plane shock wave,” Communications on Pure and Applied Mathematics **5**, 257–300 (1952), <https://doi.org/10.1002/cpa.3160050304>.
- <sup>27</sup>M. Chen and B. C. Eu, “Remarks on the modified moment method and irreversible thermodynamics,” The Journal of Chemical Physics **77**, 2696–2697 (1982), <https://doi.org/10.1063/1.444101>.
- <sup>28</sup>B. C. Eu, *Kinetic Theory and Irreversible Thermodynamics* (John Wiley and Sons, 1<sup>st</sup> edition, 1992) p. 369.
- <sup>29</sup>H. Struchtrup, *Macroscopic Transport Equations for Rarefied Gas Flows* (Springer, 2005) pp. 87–107.
- <sup>30</sup>B. C. Eu, “The modified moment method and theory of nonlinear transport processes in gases: Third order cumulant approximation,” The Journal of Chemical Physics **75**, 4031–4039 (1981), <https://doi.org/10.1063/1.442561>.
- <sup>31</sup>B. C. Eu and A. S. Wagh, “Nonlinear field dependence of carrier mobilities and irreversible thermodynamics in semiconductors,” Physical Review B **27**, 1037–1051 (1983), <https://doi.org/10.1103/PhysRevB.27.1037>.
- <sup>32</sup>B. C. Eu, “Generalized hydrodynamics approach to the Knudsen problem,” Physical Review A **40**, 6395–6402 (1989), <https://doi.org/10.1103/PhysRevA.40.6395>.
- <sup>33</sup>M. Al-Ghoul and B. C. Eu, “Generalized hydrodynamic theory of shock waves in rigid diatomic gases,” Physical Review E **64**, 046303 (2001), <https://doi.org/10.1103/PhysRevE.64.046303>.
- <sup>34</sup>B. C. Eu and Y. G. Ohr, “Generalized hydrodynamics, bulk viscosity, and sound wave absorption and dispersion in dilute rigid molecular gases,” Physics of Fluids **13**, 744–753 (2001), <https://doi.org/10.1063/1.1343908>.
- <sup>35</sup>M. Al-Ghoul and B. C. Eu, “Generalized hydrodynamics and shock waves,” Physical Review E **56**, 2981–2992 (1997), <https://doi.org/10.1103/PhysRevE.56.2981>.

- <sup>36</sup>R. S. Myong, “Thermodynamically consistent hydrodynamic computational models for high-knudsen-number gas flows,” *Physics of Fluids* **11**, 2788–2802 (1999), <https://doi.org/10.1063/1.870137>.
- <sup>37</sup>G. Garg, T. K. Mankodi, E. Esmailifar, and R. S. Myong, “Neural network-based finite volume method and direct simulation monte carlo solutions of non-equilibrium shock flow guided by nonlinear coupled constitutive relations,” *Physics of Fluids* **36**, 106113 (2024), <https://doi.org/10.1063/5.0223654>.
- <sup>38</sup>S. Zeng, W. Zhao, Z. Jiang, and W. Chen, “Computational simulation of reentry flows over hypersonic vehicles using nonlinear coupled constitutive relations,” in *AIP Conference Proceedings*, Vol. 2996 (AIP Publishing, 2024) p. 130001, <https://doi.org/10.1063/5.0187384>.
- <sup>39</sup>Z. Yuan, Z. Jiang, W. Zhao, and W. Chen, “Multiple temperature model of nonlinear coupled constitutive relations for hypersonic diatomic gas flows,” *AIP Advances* **10**, 055023 (2020), <https://doi.org/10.1063/5.0010232>.
- <sup>40</sup>T. K. Mankodi and R. S. Myong, “Boltzmann-based second-order constitutive models of diatomic and polyatomic gases including the vibrational mode,” *Physics of Fluids* **32**, 126109 (2020), <https://doi.org/10.1063/5.0026687>.
- <sup>41</sup>S. Zeng, Z. Yuan, W. Zhao, and W. Chen, “Numerical simulation of hypersonic thermochemical nonequilibrium flows using nonlinear coupled constitutive relations,” *Chinese Journal of Aeronautics* **36**, 63–79 (2023), <https://doi.org/10.1016/j.cja.2022.09.013>.
- <sup>42</sup>S. Zeng, J. Yang, W. Zhao, Z. Yuan, G. Fan, and W. Chen, “Nonlinear coupled constitutive relations for hypersonic reacting flows with thermal nonequilibrium effect,” *Physics of Fluids* **37**, 016116 (2025), <https://doi.org/10.1063/5.0249391>.
- <sup>43</sup>A. Kumar and A. S. Rana, “Capturing non-equilibrium in hypersonic flows: Insights from a two-temperature model in polyatomic rarefied gases,” *Physics of Fluids* **36**, 102007 (2024), <https://doi.org/10.1063/5.0227257>.
- <sup>44</sup>A. Kumar and A. S. Rana, “H-theorem and boundary conditions for two-temperature model: Application to wave propagation and heat transfer in polyatomic gases,” *Physical Review E* **108**, 065103 (2023), <https://doi.org/10.1103/PhysRevE.108.065103>.
- <sup>45</sup>C. Park, “Assessment of a two-temperature kinetic model for dissociating and weakly ionizing nitrogen,” *Journal of Thermophysics and Heat Transfer* **2**, 8–16 (1988), <https://doi.org/10.2514/3.55>.

- <sup>46</sup>S. P. Sharma and W. Gillespie, “Nonequilibrium and equilibrium shock front radiation measurements,” *Journal of Thermophysics and Heat Transfer* **5**, 257–265 (1991), <https://doi.org/10.2514/3.259>.
- <sup>47</sup>K. Fujita, S. Sato, T. Abe, and Y. Ebinuma, “Experimental investigation of air radiation from behind a strong shock wave,” *Journal of Thermophysics and Heat Transfer* **16**, 77–82 (2002), <https://doi.org/10.2514/2.6654>.
- <sup>48</sup>M. Furudate and K. Sawada, “Effect of rotational nonequilibrium on shock standoff distances in intermediate hypersonic range,” 39th AIAA Aerospace Sciences Meeting Exhibit, 2001–813 (2001), <https://doi.org/10.2514/6.2001-813>.
- <sup>49</sup>R. S. Myong, “On the high mach number shock structure singularity caused by overreach of maxwellian molecules,” *Physics of Fluids* **26**, 056102 (2014), <https://doi.org/10.1063/1.4875587>.
- <sup>50</sup>S. Singh, A. Karchani, K. Sharma, and R. S. Myong, “Topology of the second-order constitutive model based on the Boltzmann–Curtiss kinetic equation for diatomic and polyatomic gases,” *Physics of Fluids* **32**, 026104 (2020), <https://doi.org/10.1063/1.5133079>.
- <sup>51</sup>M. S. Liou and C. J. Steffen, “A new flux splitting scheme,” *Journal of Computational Physics* **107**, 23–39 (1993), <https://doi.org/10.1006/jcph.1993.1122>.
- <sup>52</sup>E. F. Toro, *Riemann Solver and Numerical Methods for Fluid Dynamics, A practical introduction* (Springer, 2009) p. 426.
- <sup>53</sup>J. D. Anderson, *Computational Fluid Dynamics: The Basics with Applications* (McGraw Hill, Inc., 1995) p. 131.
- <sup>54</sup>M. Camac, “Experimental measurements of shock structures,” in *Proceedings of 4th International Symposium on Rarefied Gas Dynamics* (1965) p. 240.